D1-82-0176

BOEING SCIENTIFIC RESEARCH LABORATORIES

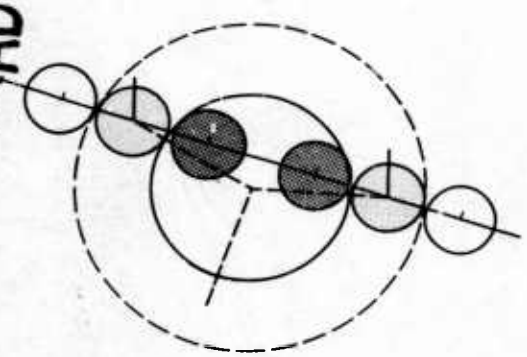

Infrared Mapping of Lunar Craters During the Full Moon and the Total Eclipse of September 5, 1960

John M. Saari

Richard W. Shorthill

July 1962

Geo-Astrophysics Laboratory

D1-82-0176

INFRARED MAPPING OF LUNAR CRATERS DURING THE FULL MOON AND THE TOTAL ECLIPSE OF SEPTEMBER 5, 1960

by

J. M. Saari
and
R. W. Shorthill
Geo-Astrophysics Laboratory
Boeing Scientific Research Laboratories
Seattle 24, Washington

July 1962

ABSTRACT

Infrared measurements were made over certain lunar crater regions during the eclipse of September 5, 1960 and the full moon. Five rayed craters were observed to cool less rapidly than their environs during the eclipse, the anomaly being greatest for Tycho and progressively less for Aristarchus, Copernicus, Proclus, and Kepler. The findings are discussed in terms of the thermal properties of the surface, including thickness of insulating layer and age of the craters. Localized variations were found during illumination, evidently attributable to variations in albedo and geometry.

ACKNOWLEDGEMENTS

The authors wish to express their gratitude to Dr. I. S. Bowen, Director of the Mount Wilson and Palomar Observatories, for his cooperation in making the facilities of the Mount Wilson Observatory available to them. The cooperation of the Observatory Staff and employees was appreciated and the authors wish to acknowledge, in particular, the helpful discussions with Dr. S. B. Nicholson and the late Dr. Edison Pettit.

The planning and preparation of the equipment and completion of the experiment would have been impossible without the invaluable assistance of Howard Borough, Richard Strissel, and George Hilt of the IR Surveillance and Mapping Group and William Nesbitt of the Nuclear Electronics Unit at Boeing.

This research was supported in part by the United States Air Force, AF 18(600)-1824 and has been reported in Boeing Document D7-2550-1 (January 30, 1961) entitled "Lunar Temperature Measurements During September 4, 5, and 6, 1960." The present paper contains revisions and data not presented in that document.

TABLE OF CONTENTS

LIST OF FIGURES

LIST OF TABLES

I. INTRODUCTION

The remarkable lunar infrared measurements of Pettit and Nicholson (1930) and Pettit (1940) provide the basis for the belief that the lunar surface material has low thermal conductivity. A homogeneous model has been discussed by Epstein (1929), Wesselink (1948), and Jaeger (1953). A two-layer model (Jaeger and Harper 1950) incorporates the cooling during an eclipse and the microwave measurements of Piddington and Minnet (1949). Further measurements of infrared cooling during an eclipse were reported by Sinton (1961). Geoffrian, Korner, and Sinton (1960) obtained infrared isotherms over the entire moon through a lunation.

During the lunar eclipse of March 13, 1960, Shorthill, Borough and Conley (1960) discovered that certain rayed craters cooled less rapidly than their environs, and in particular, that Tycho was about 40°K warmer than its environs an hour after it entered the umbra. The results for Tycho were confirmed during the September 5, 1960 eclipse by Sinton (1960) who suggested that such measurements could provide a means for dating craters.

The measurements reported here using the 60-inch telescope at Mount Wilson were designed to obtain isotherms over relatively small regions of the moon which were related to surface features. Of particular interest was the mapping of rayed craters during an eclipse to more accurately determine the extent of their anomalous cooling. Additionally, scan programs were made over a variety of crater regions

on the illuminated moon.

II. EXPERIMENTAL

a) Instrumentation

The detector was a Barnes thermistor bolometer* with an effective diameter of about 0.3mm. When mounted at the f/5 Newtonian focus, it subtended 8" of arc (about 15 km at the center of the lunar disk). The radiation detected was restricted to the infrared region beyond 2 microns by a KRS-5 window and germanium filter and was chopped at 80 cps. The amplified and synchronously rectified signal was recorded at 10 and 1 cps bandpass on two channels of a Sanborn recorder. The signal was also recorded on magnetic tape at 10 cps bandpass as an FM signal (using a modulator with a frequency of 1.2 kc and a 40 percent deviation) together with event markers (240 cps). The event markers and simultaneous vocal explanation were recorded on the other channel of the tape recorder.

The tapes were later played back and the signal demodulated using a bandpass selected to optimize the signal-to-noise ratio. By experimentation, this was found to be 0.2 cps (a time constant of about one second), which is reasonable in view of the subtended diameter of the sensor (8") and the scan motion over the surface (6"/sec). Although the data reduction was usually performed from the tape, during several scans the tape ran out and for these the original Sanborn chart record was used, the smoothing to 0.2 cps being done by eye.

---

*Barnes Engineering Co., Stamford, Connecticut

b) Scanning Technique

The scanning technique chosen was to set the clock driving the telescope in right ascension near lunar rate and then move the telescope alternately east and west with the setting motion of 6"/sec. As the moon moved north in declination, a sawtooth scan would be traced out on the lunar disk. Usually the scans were 15 seconds in each direction, so that the scans were about 90" in width; several of the scans were, however, 10 seconds and 30 seconds in each direction. The east-west scanning was timed with reference to the second hand of an electric clock, the times of reversal being noted with the event marker and by voice. Occasionally the times were lengthened or shortened in order to adjust the scan pattern. The scan paths were calculated from the time intervals between reversals, the different rates of motion in the east and west directions, and the moon's drift rate in declination. The motions were corrected for effects of parallax and atmospheric refraction by the formulas of Maxwell (1931). The scan paths and the isotherms were originally plotted to the scale 0.8" = 1 mm used for the Photographic Lunar Atlas (Kuiper 1960).

The telescope was guided with a five-inch finder scope. A mirror arrangement with an eyepiece and crosshairs at the Newtonian focus could be inserted in front of the detector; the crosshairs and detector were collimated on a star so that the mirror could be inserted at any time and the position of the detector on the lunar surface checked visually. Periodically through the night the miscollimation between the finder scope and detector would be corrected by centering

the finder crosshairs on a small lunar feature and appropriately adjusting the position of the detector; the miscollimation was usually less than 50". Although the visual position of the finder crosshairs was noted vocally on the tape, this information was used only as a rough guide for relating isotherms to surface features. Rather, when the contours drawn on translucent paper were placed over photographs from the Atlas, the positions of the isotherms with respect to the surface features were generally quite evident. Corrections were made for differences in libration.

c) Calculation of Temperatures

Since the emphasis of the experiment was on temperature differentials over localized areas, an absolute calibration of the instrument was not considered necessary. The measurements were made within a day of full moon, so a calibration was effected by periodically measuring the net subsolar point signal above sky background (Fig. 1). The net signal from other points on the moon was compared to the net subsolar point reading interpolated to the same time, this ratio of net signals, or transmitted energies, being designated by R. The subsolar point was taken to be $374^{\circ}K$ and it was assumed that the infrared energy was received through the atmospheric window simplified for purposes of calculation as shown in Fig. 2. The energy transmitted through this window from a black body at temperature T could then be compared to that calculated for 374°; by this means it was found that R could be related to T by the following empirical formula

$$\log_{10} R = 1.9435 - 776/T + 18{,}420/T^2$$

Recently Sinton (1962) has suggested a value of 389° for the temperature of the subsolar point for the moon at one A.U. from the sun. The temperatures reported here could be adjusted in accordance with this value.

The error in the observed temperature readings due to detector noise at the 0.2 cps bandpass was equivalent to ± 0.25° at 374°, ± 0.4° at 300°, and ±2.1° at 200°. However, the temperature error is probably larger than thus indicated because of reading errors and apparent slow term shifts in sky background which on several occasions (e.g. the Proclus and Menelaus scans during the full moon of September 5) yielded signals above the interpolated subsolar point reading. Sky shifts may be further evidenced on several isotherms by horizontal structure (excursions in the scanning direction). Therefore, the fine structure shown in the contours should not necessarily be interpreted as indicating real temperature differentials; it is the gross structure which should be subjected to interpretation.

III. MEASUREMENTS

Measurements were made September 4, 5, and 6, 1960 both on the illuminated moon and during the total lunar eclipse of September 5. The circumstances of this eclipse were as follows:

Moon entered penumbra	8:37 UT
Moon entered umbra	9:36
Total eclipse began	10:38
Total eclipse ended	12:06
Moon left umbra	13:08
Moon left penumbra	14:07

During the penumbral and umbral phases of the eclipse drives (i.e., single scans) were made across Aristarchus, Copernicus, and Kepler. The procedure for Aristarchus is illustrative: the telescope was centered on the crater with the guiding scope, the telescope driven east for 5 seconds, reversed, and driven west through the crater and beyond for 30 seconds. Isotherms were also made from scan programs performed during the umbral phase over the regions of Aristarchus, Copernicus, Proclus, and Tycho.

Scan programs were made over a variety of craters and their environs under illumination. TABLE 1 lists crater regions scanned during illumination and during the eclipse, and Fig. 3 shows their positions on the lunar disk.

IV. RESULTS

a) Examples of Data

An example of the demodulated and smoothed data obtained on the illuminated moon is shown by the trace in Fig. 4 obtained in the region of the crater Theophilus on September 6 at 8:47. The east and west reversing event markers are shown in the second channel; due to the finite time necessary to reverse the telescope, an offset on the chart corresponding to ~ 1.2 seconds was used for reversal points in the actual contouring. The scan path over the area is shown in Fig. 5.

b) Results on the Illuminated Moon

The structure obtained in the isotherms on the illuminated moon can be explained in terms of local differences in albedo and/or inclinations of the surface(geometry). Comments will be made

concerning the various isotherms, the craters being discussed alphabetically. The numbers in parentheses refer to the figure numbers for isotherms. On the figures the arrow shows the direction of lunar south; closed contours within which the temperature is less than outside are indicated by hachures.

Alphonsus (6,7)

The scan at 6:25 on September 5 shows some evidence of the effect of local geometry, the northern interior being 367° compared to 369° immediately outside. The temperatures at 9:23 on September 6 are generally about 3° warmer than on September 5, the effect of geometry not being as evident. There is some horizontal structure toward the southern part of Alphonsus, possibly due to a shift in sky background.

The results over Alphonsus are interesting in view of the report by Kozyrev (1959) of gaseous emission from the central peak. There is no evidence in the isotherms of a localized higher temperature in the center of the crater. However, an anomaly small compared with the subtended diameter of the sensor would not show in the contours. For instance, an anomaly 1/2 km in diameter must have a temperature of about 670° to appear as an equivalent 1° rise in temperature.

Aristarchus (8,9,10,11)

Scan programs were made under solar illumination for each of the three nights of observation. The calculation of temperature for

the isotherms made for Aristarchus, Copernicus, Kepler, and Tycho on September 4 is not considered too reliable because of inadequate subsolar point calibrations. For these isotherms, the temperature of the center of the crater was calculated using the formula

$$T = T_s \cos^{1/6} \theta$$

where θ is the angle subtended at the center of the moon between the subsolar point and the crater and T_s, the subsolar point temperature, is taken to be 374°. This empirical formula follows from the suggestion by Pettit and Nicholson (1930) that the energy variation over the surface of the full moon observed from the earth depends on $\cos^{2/3} \theta$. Temperatures at other points in the scans were calculated by comparing the deflections to that obtained at the crater.

The isotherms over Aristarchus on September 4 show the effects of geometry: the illuminated eastern interior slope is warmer than the western interior slope. The isotherms for 6:57 on September 5 show a cooler area in the region of the crater of about 2°. There is evidence of a considerable amount of structure in the direction of the scan which largely disappears in the "rectified" contour shown in Fig. 11; here the effect of the moon's curvature in producing a temperature gradient in the direction of the subsolar point has been removed keeping the temperature at the center of Aristarchus the same. For the isotherms of September 6 (Fig. 10) the effect of albedo is more apparent since the crater appears to be 4° cooler than the environs. The cooler area around Aristarchus extends toward Herodotus.

Cleomedes (12)

Although the scan pattern did not cover all of the crater Cleomedes, the strong influence of geometry is evident over this crater and the neighboring craters Tralles and part of Burkhardt. On this scan and several others, the isotherms were not contoured to integral values of temperature.

Copernicus (13,14,15)

Scan programs were made on the illuminated crater each night. Interestingly enough, the effect of geometry is most clearly shown for September 5 where there is a temperature differential of 4° to 5° between the eastern and western interior slopes. The large loop around the crater for the 370° contour on September 6 shows an increasing effect of albedo. The high indicated temperatures for the September 4 isotherms can be attributed to the method of calibration; the direction of the general temperature gradient is toward the northwest, rather than that expected, toward the west-southwest direction.

Dionysius (16)

The general thermal structure here apparently is not well related to visible features except for Dionysius itself, which appears to be cooler than its environs by 3° to 4° by reason of its higher albedo. This anomaly extends beyond the crater and is comparable in area to the lighter region around the crater. The horizontal structure is evidence of shifts in the sky background.

Kepler (17)

This scan shows the general gradient expected without any

particular correlation of the isotherms with the crater. In this case the visual position of the crater is indicated since it was not possible to match the isothermal contours with features. The error in the position is probably not more than 10" or 20".

Menelaus (18)

The temperatures calculated here are higher than the assumed subsolar point temperature, which may indicate a shift in sky background. This may be indicated additionally by the horizontal structure at the bottom of the figure. Nonetheless, the albedo effect in the region of this bright crater is clearly evident, extending beyond the crater.

Posidonius (19)

The geometrical effects are not very pronounced in these isotherms over the region of Posidonius, the general gradient from the subsolar point being the main feature evident.

Proclus (20,21)

Both of the isotherms are characterized by an enhanced temperature gradient near the boundary between the ray system of Proclus and Palus Somnii. Variations over Proculus on September 5 are not as evident as on September 6. There is an area on the eastern edge of Mare Crisium on September 6 which is 2° or 3° cooler than its environs. The isotherms for September 5 include temperatures higher than that assumed for the subsolar point.

Theophilus (22)

The isotherms reveal structure due to geometry over the craters Theophilus, Cyrillus, and Catharina. For instance, the more directly illuminated western interior slope of Theophilus is 365.7° compared to 358.5° for the eastern interior slope.

Tycho (23,24,25)

The isotherms over Tycho show evidence of the effect of geometry on temperature. The isotherms for September 5 show variations in craters Pictet and Street; the western interior of Longomontanus is cooler than the eastern interior.

c) Results During the Eclipse of September 5, 1960

Drives were made across Aristarchus, Copernicus, and Kepler at various times during the penumbral phase of the eclipse, and across the first two during the umbral phase (it was difficult to observe Kepler then). Additionally, scan programs were made over the regions of Aristarchus, Copernicus, Proclus, and Tycho during the umbral phase.

Tracings of the original data for drives across Aristarchus, Copernicus, and Kepler are shown in Figs. 26, 27, and 28. In the early part of the penumbra Aristarchus appears to be cooler than its environs while later it appears warmer. Similar anomalies are exhibited by Copernicus and Kepler.

Isotherms over Aristarchus (Figs. 29 and 30) reveal the extent of the anomaly during the umbral phase. The isotherms for 10:12

show the center of the crater to be 228° whereas its environs are 203°. At 11:04 considerable horizontal structure is evident; the anomaly nonetheless is clearly shown, the indicated temperature at the crater being 231° compared to 207° for its environs.

The isotherms over Copernicus (Fig. 31) for 11:30 show horizontal structure. The anomaly is revealed in the area where the temperature rises above 230° compared to an environs temperature of perhaps 210°. At this time the anomaly does not seem to extend significantly beyond this crater.

In order to determine if other rayed craters exhibit the anomalous eclipse cooling, a scan program was made over Proclus at 11:56. In the isotherms a differential of 12° is indicated, the crater being 222° compared to 210° for its environs.

Measurements were also made over Tycho at 10:34 (Fig. 33) in which the previously reported anomalous cooling was mapped to reveal its extent on the lunar surface. There is a 31° differential between the crater and its environs, the crater being 243° and the environs 212°. Again, the anomaly extends beyond the crater.

The results of the cooling measurements made on Aristarchus, Copernicus, and Kepler both from the drives and isotherms are shown in Figs. 34, 35, and 36. The fluctuations in the data during the umbral phase (in the Aristarchus data for example) are probably caused by sky background fluctuations. This causes the temperature differentials observed during the umbral phase to vary from 21° to

44° (Fig. 37). If, however, the difference in observed energy ratios between the crater and its environs is plotted instead of the temperatures, sky fluctuations will not be so evident (Fig. 38). Initially, the crater center is cooler than the environs with $\Delta R = -0.044$. At about 0.2 the way through the penumbra phase ΔR is zero, indicating equal temperatures, and by the time 0.8 of the penumbral phase has passed, ΔR has reached an equilibrium value which apparently is maintained as long as measurements were made, the average value during this time being $\Delta R = 0.048$.

In TABLES 2 through 8 are presented the cooling data for Aristarchus, Copernicus, Kepler, their environs, and a point 166" west of Aristarchus. The results are given in terms of time and temperature (TABLES 2 through 4), and in terms of data normalized to initial temperature T_o and time spent in penumbra t_o (TABLES 5 through 8).

V. DISCUSSION

The temperature variations obtained on the illuminated moon can be accounted for by variations in local albedo and the geometrical effect of the inclination of surfaces with respect to the sun. Wesselink (1948) has pointed out that the conductive component into the interior (which depends on the thermal properties of the surface) is important only during the lunar night or near local sunrise or sunset.

The effect of albedo is illustrated by the isotherms obtained over Menelaus (Fig. 18), the interior of the crater being 384° and its environs 390°. Defining the absorptance as the ratio of absorbed energy (measured as planetary heat) to that incident, we can calculate that the ratio of absorptance in the crater to its environs will be $(384/390)^4$ or 0.94. Such calculations will depend on the phase of the moon and the location of the area. Infrared measurements through a lunation on selected areas will provide a means for studying the relationship between the radiometric function and the photometric function as discussed by van Diggelen (1959). For instance, he pointed out that the rayed craters Aristarchus, Copernicus, and Tycho attain their maximum brightness at a phase angle 10° after full moon. It is interesting that the isotherms for Aristarchus made on September 6 at a phase angle of 10° after full moon show effects of albedo more than those made previously on September 4 or 5.

The effect of geometry on observed full moon temperatures can be calculated using the formula $T = T_s \cos^{1/6} \theta$ where θ now is the angle between the normal to the surface and the direction of the sun. This will be illustrated by calculating the temperature ratio between the interior slopes closest and farthest from the subsolar point for two craters. For the isotherms made over Copernicus on September 5, the angle to the subsolar point was 28.8°, predicting a temperature for a level area at the crater of 365.9°. This agrees

with an observed temperature of 365.5° for the interpolated environs; the center of the crater was found to be 362°, which is brighter and should be cooler. The interior slopes were estimated from the contour elevations shown on the U.S.A.F. Lunar Chart LAC 58 (1st edition, July 1961) to be 11.0 degrees on the side closest to the subsolar point and 9.3 degrees for the side farthest away. With the curvature of the moon taken into account, the more directly illuminated slope should be 3.0% warmer than the opposite slope. This is to be compared with observed values of 364.2° and 360.0°, a difference of only 1.2%. Similarly, calculations for Theophilus, using the profile data of McMath, Petrie and Sawyer (1931), predict a different of 3.8% compared to observed values of 365.7° and 358.5°, a difference of only 2.0%. The calculated temperature for a level area at Theophilus is 361.5° which is quite close to the average of the above two values. From these measurements it appears that the formula is satisfactory in predicting the temperature for a level area at the craters; however, the observed values of the ratio of temperatures on the interior slopes do not agree with predicted values. Although instrumental effects such as the finite size of the sensor and the smoothing used on the temperature signal may account for some of the discrepancy, it is possible that the interior surfaces of craters have a different structure than other parts of the moon so that a different roughness factor is operative.

The anomalous eclipse cooling of the rayed craters will be

discussed first in terms of the actual measurements, and second with reference to several models. In TABLE 9 are listed the energy ratios for the five rayed craters and their interpolated environs before the eclipse, R_o, and during the umbra, R_f. These ratios were taken from isotherms except in the case of Kepler where the results from the drive just as it entered the umbra were used. Although the values of R are sensitive to fluctuations in sky background, the difference in R_f between the crater and its environs should be less sensitive (since the measurements were made seconds apart in time). The craters have been ordered in the table according to decreasing ΔR_f, Tycho exhibiting the largest anomaly for this parameter, with Aristarchus, Copernicus, Proclus, and Kepler showing a progressively smaller discrepancy. Shown also are R_f/R_o and the corresponding values of $\Delta (R_f/R_o)$ between the craters and their environs (the latter parameter is normalized for different initial values of R_o).

The cooling curves for Aristarchus, Copernicus, and Kepler are plotted in Figs. 39 through 44 in terms of normalized coordinates, that is, temperature compared to initial temperature and time compared to the time spent in the penumbra. In the first three figures the theoretical curves of Jaeger (1953) for the one-layer model are shown with values of $(K\rho c)^{-1/2}$ corresponding to the different values of T_o and t_o. On the last three figures the results of Jaeger and Harper (1950) for the two-layer model are

shown. The fall in temperature calculated for this eclipse for a surface with zero conductivity is also plotted. The environs of Aristarchus and a point in the mare near Diophantus 166" west in right ascension from Aristarchus parallel the insolation curve during the penumbra, whereas the center of Aristarchus initially seems to stay above the other curves. The data during the umbra for Copernicus and Aristarchus show considerable scatter, but may indicate a better agreement with the two-layer model than with the one-layer model.

The rayed craters, thought to be younger features of the moon, may have a thinner dust layer than their environs because of the shorter period for accumulation of the layer by meteoric infall. In interpreting his results for Tycho during the September 5, 1960 eclipse, Sinton (1960) calculated the dust thickness d using the expression

$$\sigma T_f^4 = K (T_{ss} - T_f)/d$$

where T_f is the temperature of the crater during totality, T_{ss} the temperature of the upper surface of the substratum, and K the thermal conductivity of the layer (assumed to be 2.8×10^{-6} cal cm^{-1} deg^{-1} sec^{-1}). This formula fits the theoretical eclipse results for the two-layer model of Jaeger and Harper (1950) if T_{ss} is taken to be 0.73 times the initial surface temperature T_o of the crater. The temperature data and calculated dust thicknesses

for the five rayed craters are shown in TABLE 10, ranging from 0.075 mm for Tycho to 0.71 mm for Kepler. The age τ of a crater, assuming a constant accretion rate $\dot{m}$ of meteoric material per unit area on the lunar surface, is given by

$$\tau = \rho d/\dot{m}$$

where ρ is the density of the layer. If $\dot{m}$ is calculated from the accretion rate $\dot{M}$ on the entire earth taking into account the ratio of the areas of the earth and moon and an additional factor of 30 percent because of the higher gravitational field of the earth (Brown 1960), the age becomes

$$\tau = 1820\ \rho d/\dot{M} \quad \text{(million years)}$$

where ρ is in g/cm^3, d in mm, and $\dot{M}$ in tons/day. Dubin and McCracken (1962) have estimated $\dot{M}$ to be of the order of 10^4 tons/day; with ρ assumed to be 2 g/cm^3, the age of Tycho is 0.027 m.y. from our thickness data. Whipple (1960) estimated M to be of the order of 10^3 tons/day; the ages for the craters using this more conservative value are shown in TABLE 10, and range from 0.27 m.y. for Tycho to 2.6 m.y. for Kepler.

The absolute ages of the craters are subject to some uncertainty, not only because the accretion rate for the moon is not well known, but also because the formation of a layer on the moon by meteoric infall is undoubtedly a more complex process than

assumed above. For example, Jaeger and Harper estimate the thickness of the dust layer on the moon to be of the order of 2 mm: it would require only 7 m.y. to build up this thickness using Whipple's data, and only 0.7 m.y. using Dubin and McCracken's data! Van Diggelen (1959) has suggested that the albedo of the rayed craters may be an indication of their age; in TABLE 10 are also listed his values of the normal albedo and phase lag after full moon to reach maximum brightness. Although these different parameters do not order in the same way, such comparative measurements may prove useful in understanding the mode and sequence of crater formation.

The anomalous cooling possibly may be explained by a local subsurface temperature excess. For example, by assuming the same dust layer over the environs (with a substratum temperature during totality equal to 0.73 times the surface value before entering the penumbra) as over the craters, it is possible to calculate the substratum temperature for the craters to account for the higher measured umbral temperature. Expressed as a fraction of the initial crater temperature, the values calculated were 0.92 for Tycho, 0.90 for Aristarchus, 0.83 for Copernicus, 0.81 for Proclus, and 0.79 for Kepler, compared to the value 0.73 assumed for the environs.

Recently Buettner (1962), referring to the eclipse cooling data on Aristarchus, has suggested that the higher umbral temperatures may be explained by a greater transparency of the surface for the infrared in the craters compared to the environs, so that the

detector sees warmer deeper layers. Other interpretations may be possible; unfortunately, the eclipse measurements do not unambiguously define the local lunar surface in terms of the several models postulated. Measurements over rayed craters during the lunar night would be valuable in ascertaining whether the anomalies persist over a longer cooling period; infrared spectroscopy from balloons would yield valuable information on the details of infrared emission by the lunar surface.

VI. CONCLUSIONS

The isotherms over various crater areas near full moon show variations due to localized differences in albedo and geometry. Regarding geometry, the $T_s \cos^{1/6} \theta$ law reasonably predicts the temperatures of a level area in the regions of Theophilus and Copernicus. There is, however, a discrepancy between the predicted and measured ratios of temperature for the interior slopes nearest and farthest from the subsolar point for these craters. Several isotherms over Alphonsus do not reveal a temperature anomaly over the central peak (where gaseous emission has been reported); however, an anomaly small compared to the projected area of the sensor would not necessarily be noticeable.

The five rayed craters Tycho, Aristarchus, Copernicus, Proclus and Kepler cooled less rapidly during the eclipse than their environs. The anomalies were greatest near the center of the crater and extended

beyond the crater. Interpreted in terms of dust thickness, the results may provide a means of dating these craters, the calculations indicating age values ranging from 0.27 m.y. for Tycho to 2.6 m.y. for Kepler.

VII. REFERENCES

Brown, H. 1960, J. Geophys. Research, 65, 1679.

Buettner, K. J. K. 1962, Rand Document RM-3263-JPL, September.

Diggelen, J. van 1959, Rech. Obs. Utretcht, 14, No. 2.

Dubin, M. and McCracken, C. W. 1962, Astron. J., 67, No. 5, 248.

Epstein, P. S. 1929, Phys. Rev., 33, 269.

Geoffrion, A. R., Korner, M., and Sinton, W. M. 1960, Lowell Obs. Bull., 5, No. 1, 1.

Jaeger, J. C. 1953, Australian J. Phys., 6, 10.

Jaeger, J. C. and Harper, A. F. A. 1950, Nature, 166, 1026.

Kuiper, G. P. 1960, ed., Photographic Lunar Atlas (University of Chicago Press, Chicago).

Kozyrev, N. A. 1959, Sky and Telescope, 18, No. 4, 184.

Maxwell, A. D. 1931, Pub. Obs. U. of Michigan, 4, No. 4, 66.

McMath, R. R., Petrie, R. M., and Sawyer, H. E. 1937, Publ. Obs. U. of Michigan, 6, No. 8, 67.

Pettit, E. 1940, Ap. J., 91, 408.

Pettit, E. and Nicholson, S. B. 1930, Ap. J., 71, 102.

Piddington, J. H. and Minnett, H. C. 1949, Australian J. Sci. Res., 2, 63.

Shorthill, R. W., Borough, H. C., and Conley, J. M. 1960, Pub. A.S.P., 72, 481.

Sinton, W. M. 1960, Lowell Obs. Bull., 5, No. 3, 25.

Sinton, W. M. 1961, Planets and Satellites, ed. G. P. Kuiper and B. M. Middlehurst (University of Chicago Press, Chicago).

Wesselink, A. J. 1948, B.A.N., 10, 351.

Whipple, F. L. 1960, The Exploration of Space, ed. R. Jastrow (Macmillan, New York).

TABLE 1

CRATER REGIONS SCANNED

	UT	Figs.
September 4, 1960		
Tycho	10:08	23
Copernicus	10:20	13
Aristarchus	10:30	8
Kepler	10:37	17
September 5, 1960		
Tycho	5:18	24
Copernicus	5:48	14
Alphonsus	6:25	6
Aristarchus	6:57	9-10
Proclus	7:20	20
Menelaus	7:44	18
*Aristarchus	10:12	29
*Tycho	10:34	33
*Aristarchus	11:04	30
*Copernicus	11:30	31
*Proclus	11:56	32
September 6, 1960		
Tycho	5:50	25
Copernicus	6:27	15
Aristarchus	6:56	11
Cleomedes	7:33	12
Proclus	7:54	21
Dionysius	8:12	16
Theophilus	8:47	22
Alphonsus	9:23	7
Posidonius	10:34	11

*During eclipse

TABLE 2

ECLIPSE CODING DATA FOR ARISTARCHUS

Time September 5, 1960	Temperature (°K)		
	Crater	Environs	166" West
8:30.0	~ 350	~ 354	
(Enters Penumbra)	(8:48.1)*	(8:48.1)*	(8:52.3)*
8:52.9	350	354	
8:54.6	351		
8:57.8	349	347(d)	
8:58.7			361
9:00.1			362
9:00.9	350	349	
9:01.7	346	345	
9:03.3	343(1)		
9:04.2	342	340	
9:04.6			354
9:05.0	340	339	
9:05.8	342	339	
9:06.2			355
9:08.6	337(d)	335(d)	
9:09.0			351
9:09.4	337	335	
9:10.2	334	332	
9:10.6			348
9:12.2	331	329	
9:12.6			345
9:14.0			342
9:38.6	266	253	
9:39.0			274
9:40.8	254	235	
9:41.2			264
9:41.6	251	235	
9:42.3	250	234	
9:42.8			259
(Enters Umbra)	(9:52.5)*	(9:52.5)*	(9:57.1)*
9:55.8	222	182	
9:56.6			202
10:00.2	219	182	
10:01.8	227	186	
10:07.0	225	181	
10:12.2	225	205	
10:14.6	224	189	
10:44.7	231	204	
10:52.7	229	200	
10:58.0	230	200	200
11:10.7	223		

* time
(1) reading may be low
(d) doubtful reading

TABLE 3

ECLIPSE COOLING DATA FOR COPERNICUS

Time September 5, 1960 UT	Temperature (°K)	
	Crater	Environs
8:30.0 (Enters Penumbra)	361 (8:53.8)*	365 (8:53.8)*
9:19.0	346	345
9:20.5	346	343
9:25.2	332	331
9:28.5	321	297
9:31.5	315	313
9:43.7	269	269
9:46.9	258	254
9:53.8 (Enters Umbra)	230 (9:56.5)*	225 (9:56.5)*
11.30.0	225	210

*time

TABLE 4

ECLIPSE COOLING DATA FOR KEPLER

Time September 5, 1960 UT	Temperature (°K)	
	Crater	Environs
8:30.0 (Enters Penumbra)	~ 359 (8:46.2)*	~ 359 (8:46.2)*
9:23.5	304	302
9:23.8	306	303
9:26.7	297	296
9:30.2	290	286
9:33.2	279	272
9:45.3 (Enters Umbra)	229 (9:48.9)*	218 (9:48.9)*
9:49.2	203	194

*time

TABLE 5

NORMALIZED COOLING DATA FOR ARISTARCHUS

Crater Initial Temp. T_o = 350 °K Time in Penumbra t_o = $64^m.4$				Environs Initial Temp. T_o = 354 °K	
Time t	t/t_o	Temp. T (°K)	T/T_o	Temp. T (°K)	T/T_o
4.8	0.074	350	1.000	354	1.000
6.6	0.102	351	1.002		
9.7	0.151	349	0.997	347	0.980
12.8	0.199	350	1.000	349	0.986
13.6	0.211	346	0.988	345	0.974
15.2	0.236	343	0.980		
16.3	0.253	342	0.977	340	0.960
16.9	0.262	340	0.971	339	0.958
17.7	0.274	342	0.977	339	0.958
20.5	0.318	337	0.963	335	0.949
21.3	0.331	337	0.963	335	0.949
22.1	0.343	334	0.954	332	0.938
24.1	0.374	331	0.946	329	0.929
50.5	0.784	266	0.760	253	0.715
52.7	0.818	254	0.726	235	0.664
53.5	0.831	251	0.717	235	0.664
54.2	0.842	250	0.714	234	0.661
67.7	1.051	222	0.634	182	0.514
72.1	1.120	219	0.626	182	0.514
73.7	1.144	227	0.648	186	0.525
78.9	1.225	225	0.643	181	0.511
84.1	1.305	225	0.643	205	0.579
86.5	1.343	224	0.640	189	0.534
96.6	1.500	231	0.660	204	0.576
124.6	1.935	229	0.654	200	0.565
129.9	2.017	230	0.657	200	0.565
142.6	2.214	233	0.637		

TABLE 6

NORMALIZED COOLING DATA FOR A POINT 166" WEST OF ARISTARCHUS

Time		166" West of Aristarchus Near Diophantus Initial Temp. T_o = 362°K Time in Penumbra t_o = $64^m.8$	
t from start of penumbra	t/t_o	Temp. T (°K)	T/T_o
$6^m.4$	0.099	361	0.997
7.8	0.120	362	1.000
12.3	0.190	354	0.978
13.9	0.214	355	0.981
16.7	0.258	351	0.970
18.3	0.282	348	0.961
20.3	0.313	345	0.953
21.7	0.335	342	0.945
46.7	0.721	274	0.757
48.9	0.755	264	0.729
50.5	0.779	259	0.715
68.5	1.057	202	0.558
125.7	1.940	200	0.552

TABLE 7

NORMALIZED COOLING DATA FOR COPERNICUS

Time		Crater Initial Temp. T_o = 361°K Time in Penumbra t_o = $62^m.7$		Environs Initial Temp. T_o = 365°K	
t from start of penumbra	t/t_o	Temp. T (°K)	T/T_o	Temp. T (°K)	T/T_o
$25^m.2$	0.402	346	0.958	345	0.945
26.7	0.426	346	0.958	343	0.940
31.4	0.501	332	0.920	331	0.907
35.0	0.558	321	0.889	297	0.814
37.7	0.601	315	0.872	313	0.858
49.9	0.796	269	0.745	269	0.737
53.1	0.847	258	0.715	254	0.696
60.0	0.957	230	0.637	225	0.616
156.2	2.491	225	0.623	210	0.575

TABLE 8

NORMALIZED COOLING DATA FOR KEPLER

Time		Crater Initial Temp. $T_o = 359^oK$ Time in Penumbra $t_o = 62^m.7$		Environs Initial Temp. $T_o = 359^oK$	
t from start of penumbra	t/t_o	Temp. T (^oK)	T/T_o	Temp. T (^oK)	T/T_o
$37^m.3$	0.595	304	0.847	302	0.841
37.6	0.600	306	0.852	303	0.844
40.5	0.646	297	0.827	296	0.824
44.0	0.702	290	0.808	286	0.800
47.4	0.756	279	0.777	272	0.758
59.1	0.943	229	0.638	218	0.607
63.0	1.004	203	0.565	194	0.540

TABLE 9

ANOMALOUS COOLING OF RAYED CRATERS IN TERMS OF MEASURED QUANTITIES

R_o = initial ratio R_f = final ratio	Crater				
	Tycho	Aristarchus	Copernicus	Proclus	Kepler
Crater R_o	0.751	0.751	0.862	0.924	0.842
R_f	0.116	0.079	0.072	0.066	0.037
R_f/R_o	0.154	0.105	0.084	0.072	0.044
Environs R_o	0.771	0.791	0.905	0.936	0.842
R_f	0.049	0.037	0.046	0.046	0.027
R_f/R_o	0.064	0.047	0.051	0.049	0.032
ΔR_f(crater-environs)	0.067	0.042	0.026	0.020	0.010
$\Delta(R_f/R_o)$(crater-environs)	0.090	0.058	0.033	0.022	0.012

TABLE 10

ANOMALOUS COOLING OF RAYED CRATERS IN TERMS OF DERIVED PARAMETERS

T_o = initial temperature T_f = final temperature d = thickness of insulating layer		Crater				
		Tycho	Aristarchus	Copernicus	Proclus	Kepler
Crater	T_o	350	350	361	367	359
	T_f	243	228	225	222	203
	T_f/T_o	0.69	0.65	0.62	0.60	0.57
Environs	T_o	352	354	365	368	359
	T_f	212	203	210	210	194
	T_f/T_o	0.60	0.57	0.58	0.57	0.54
ΔT_f(Crater-environs)		31	25	15	12	9
$\Delta(T_f/T_o)$		0.092	0.078	0.048	0.035	0.026
d(crater)mm		0.075	0.21	0.31	0.39	0.71
d(environs)mm		0.46	0.67	0.60	0.63	0.99
d(crater)/d(environs)		0.16	0.31	0.52	0.62	0.72
Crater age m.y.*		0.27	0.76	1.1	1.4	2.6
Albedo		0.131	0.152	0.114	0.142	0.102
Phase angle of maximum radiance		10°	10°	10°	5°	8°

*Assuming meteoric accretion rate on earth is 10^3 tons/day.

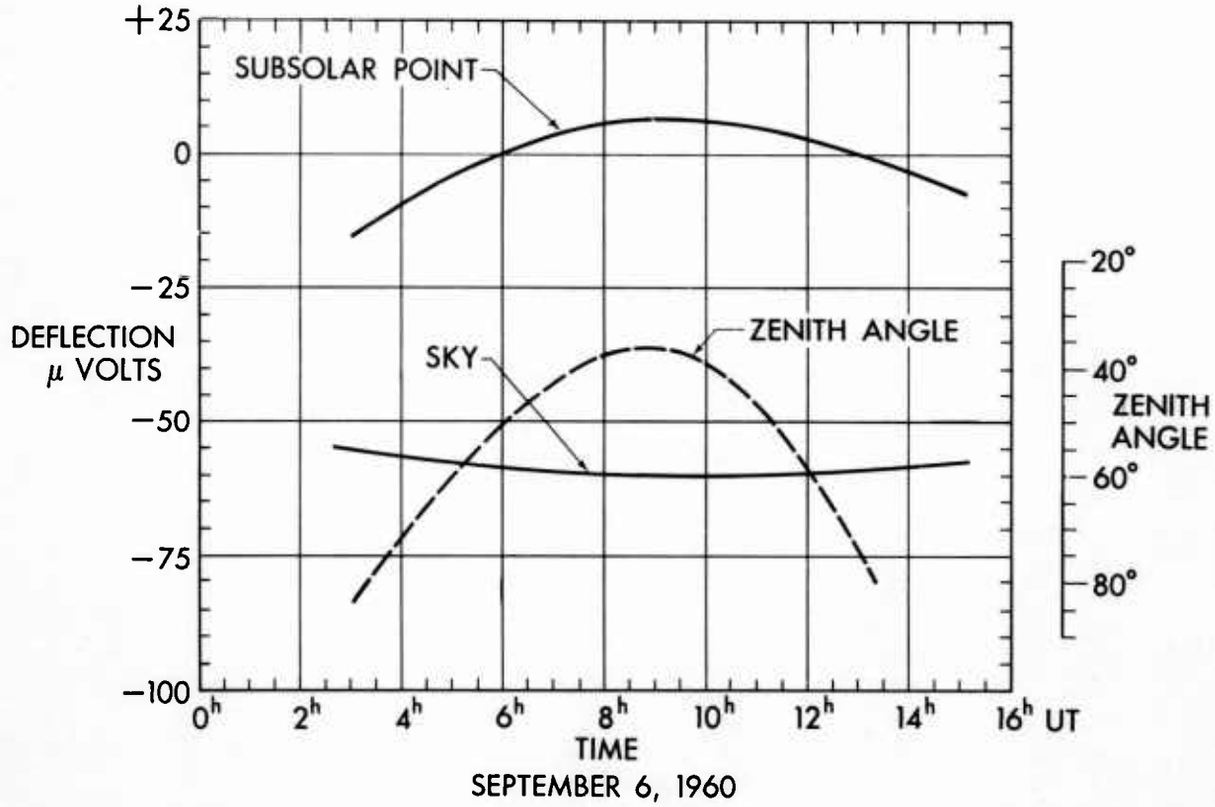

Fig. 1. Calibration Curves From Sky and Subsolar Point Readings

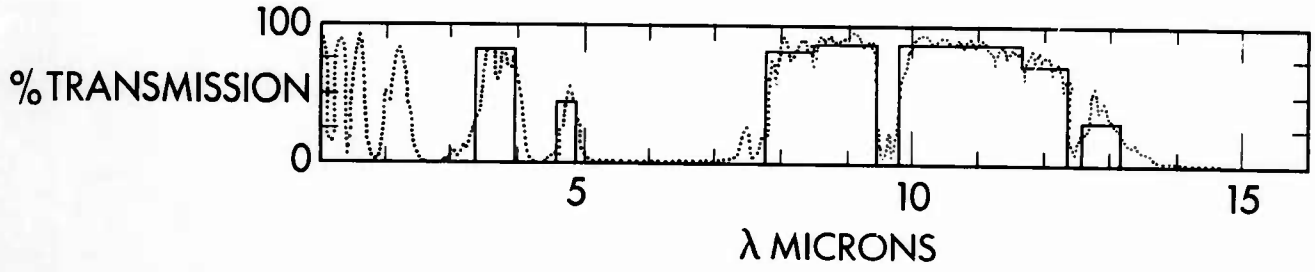

Fig. 2. Simulated Atomspheric Transmission Curve

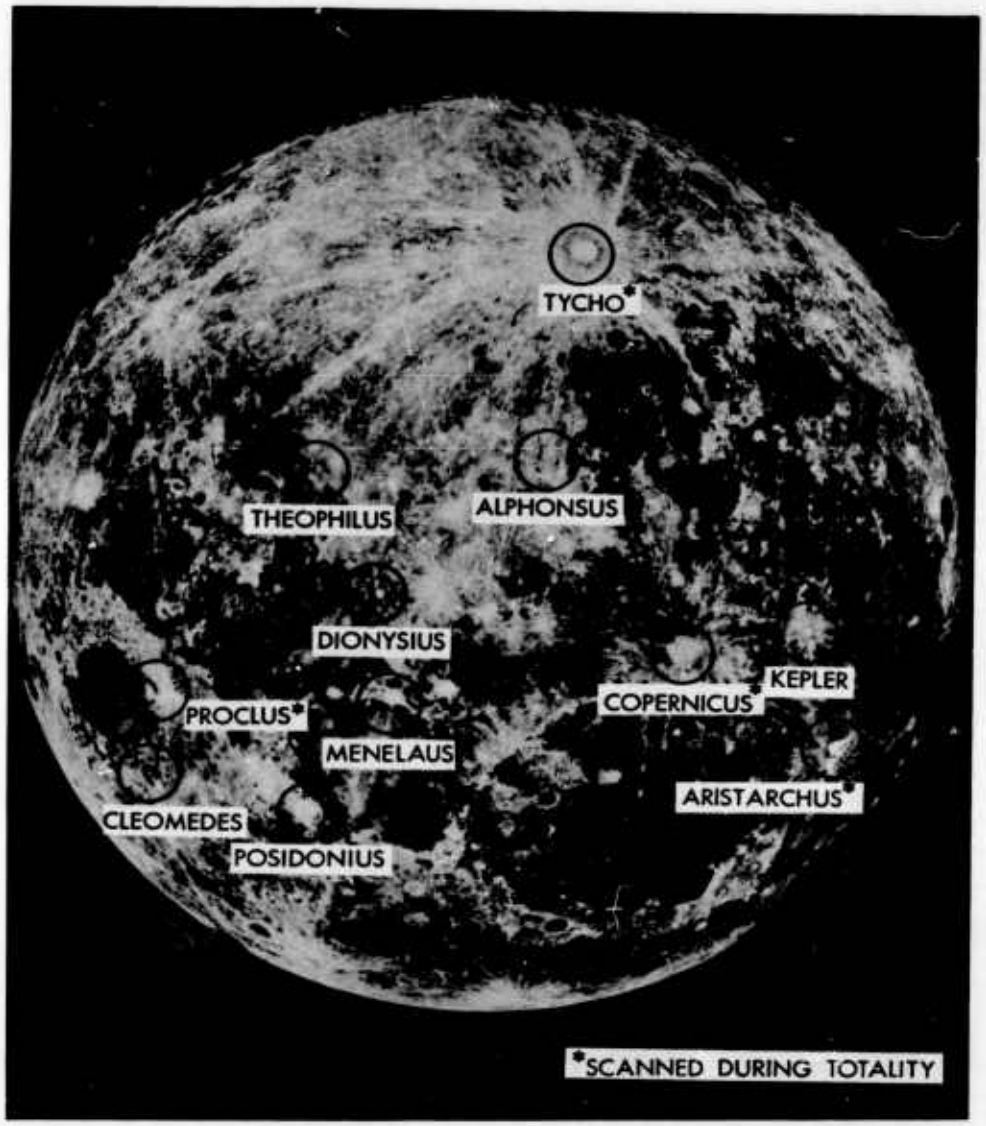

Fig. 3. Crater Areas Scanned September 4, 5, and 6, 1960

Photograph Courtesy Lick Observatory

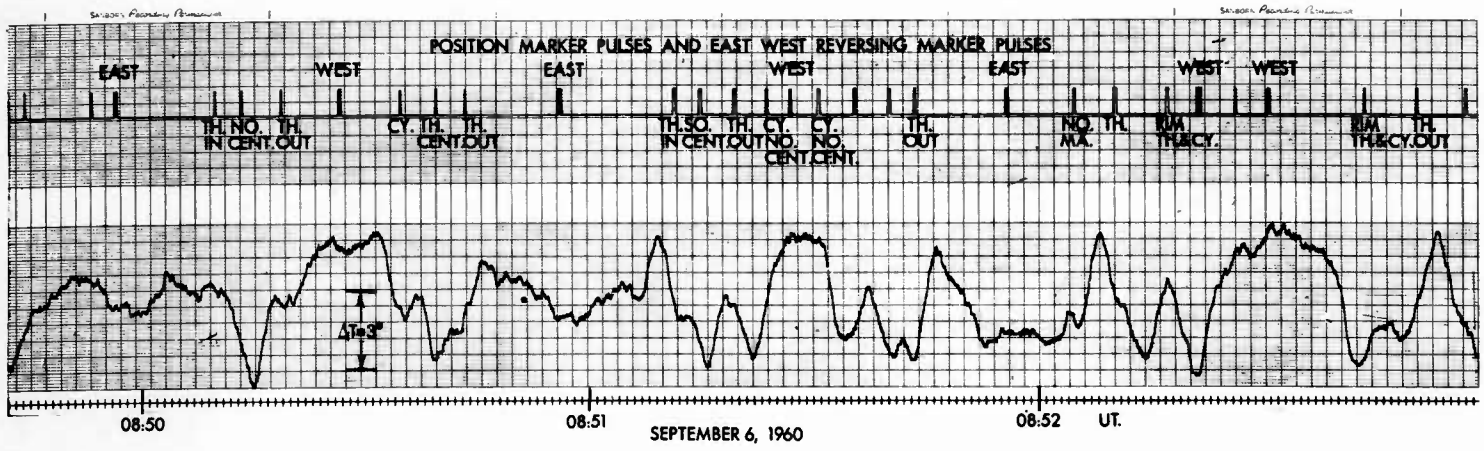

(TH.=THEOPHILUS, CY.=CYRILLUS, MÄ.=MÄDLER,
NO.=NORTH, SO.=SOUTH, CENT.=CENTER)

Fig. 4. Demodulated Temperature Traces Over Theophilus and its Environs Using a Time Constant of One Second

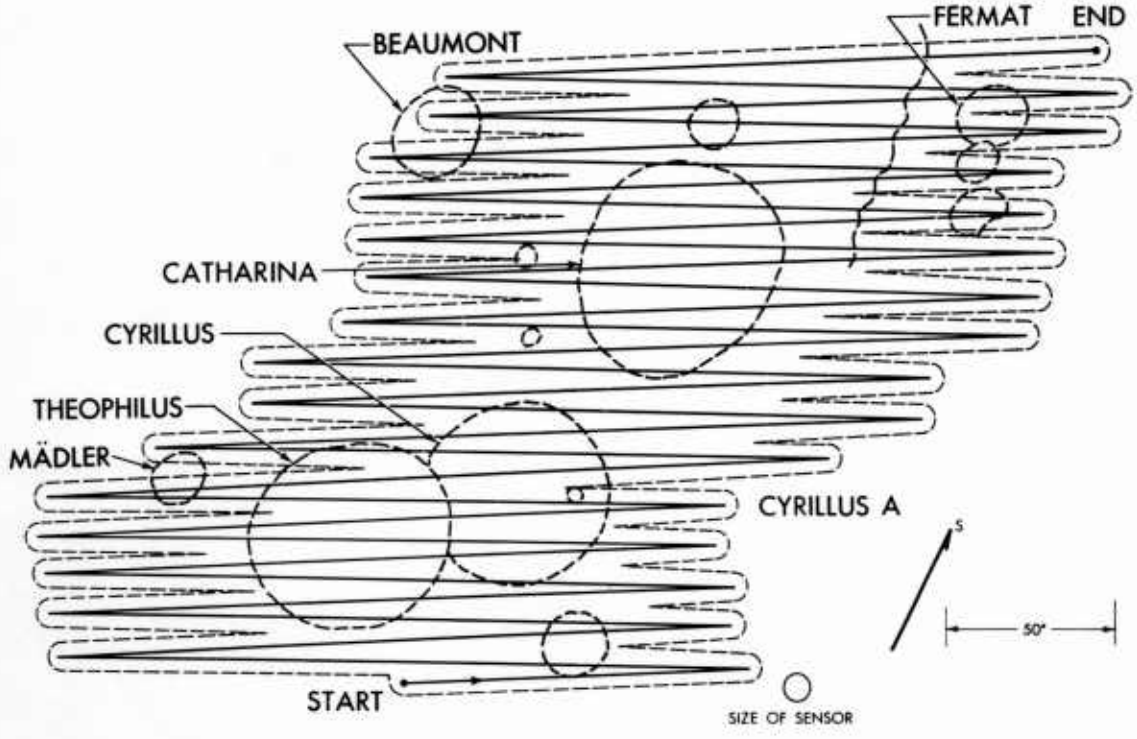

Fig. 5. Scan Path in the Region of Theophilus September 6, 1960, 8:47 UT

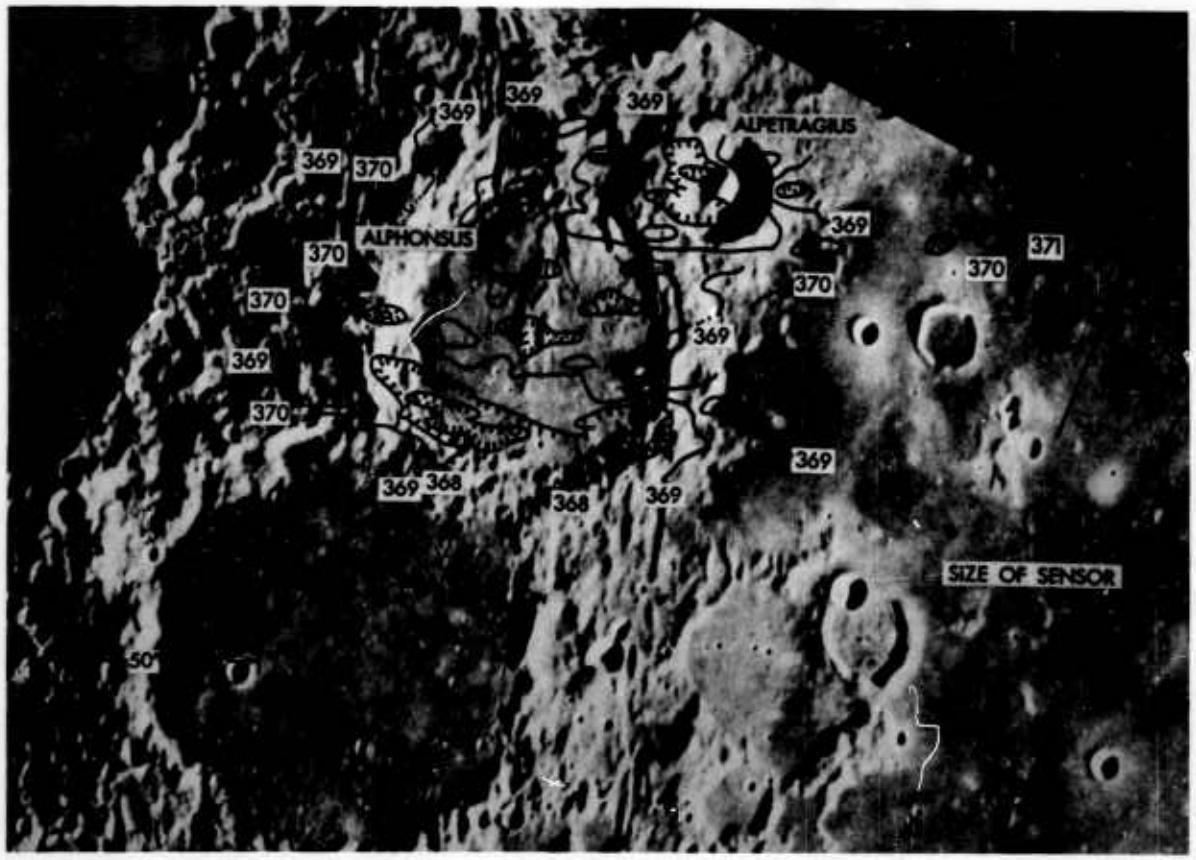

Fig. 6. Isotherms in the Region of Alphonsus September 5, 1960, 6:18 UT

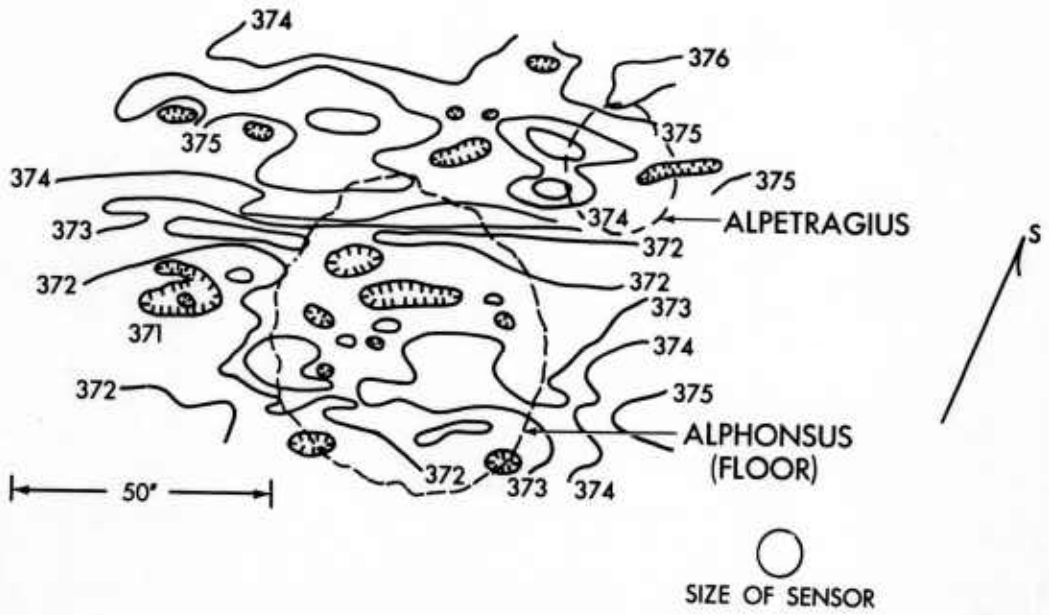

Fig. 7. Isotherms in the Region of Alphonsus September 6, 1960, 9:23 UT

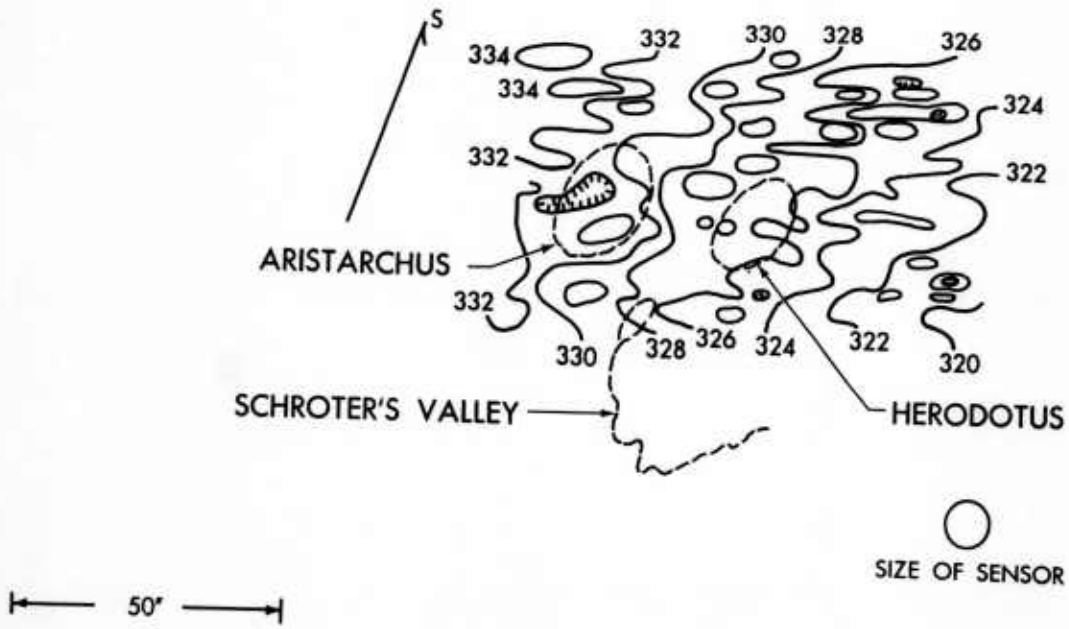

Fig. 8. Isotherms in the Region of Aristarchus September 4, 1960, 10:30 UT

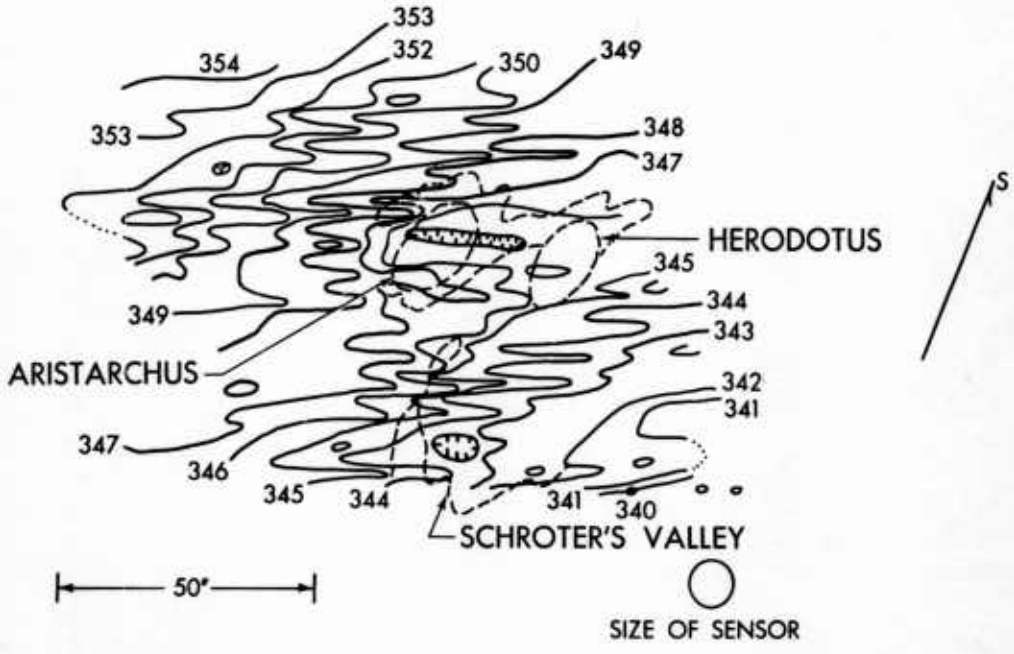

Fig. 9. Isotherms in the Region of Aristarchus September 5, 1960, 6:57 UT

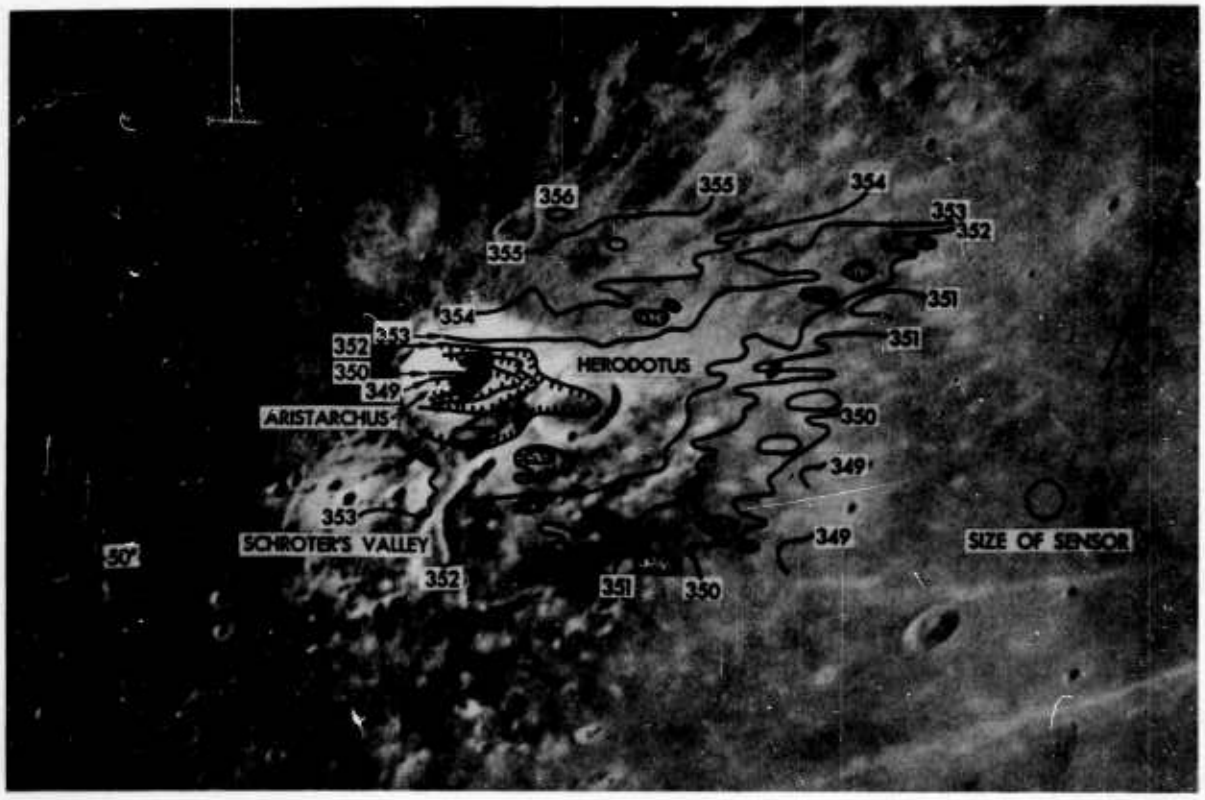

Fig. 10. Isotherms in the Region of Aristarchus September 6, 1960, 6:56 UT

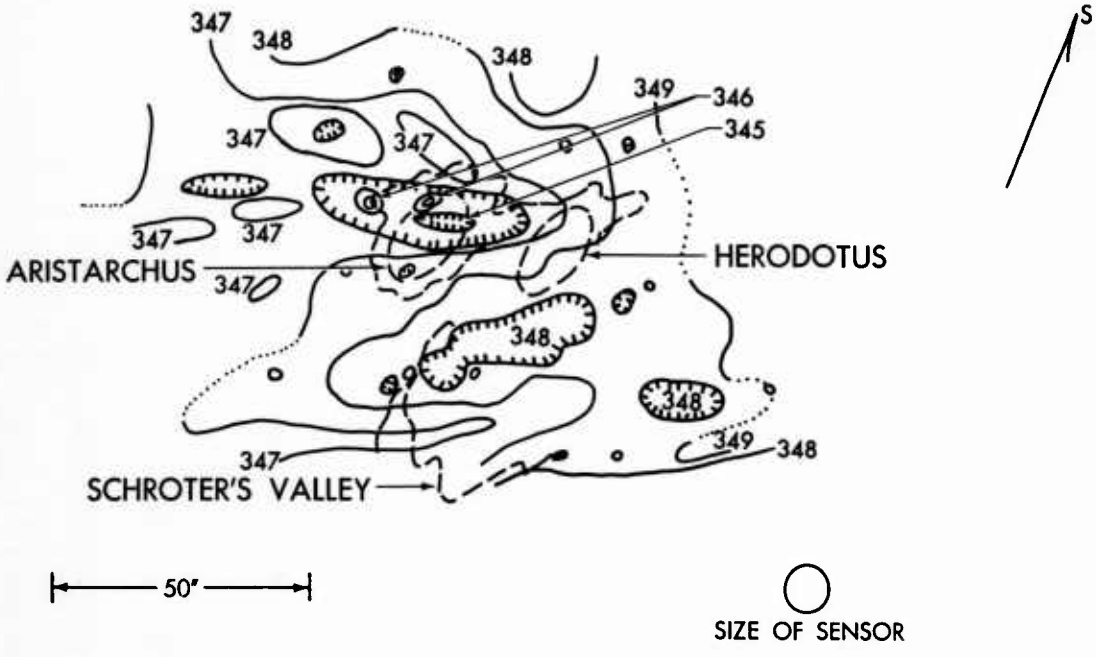

Fig. 11. Isotherms in the Region of Aristarchus Rectified to Remove the Effect of the Curvature of the Surface, September 5, 1960, 6:57 UT

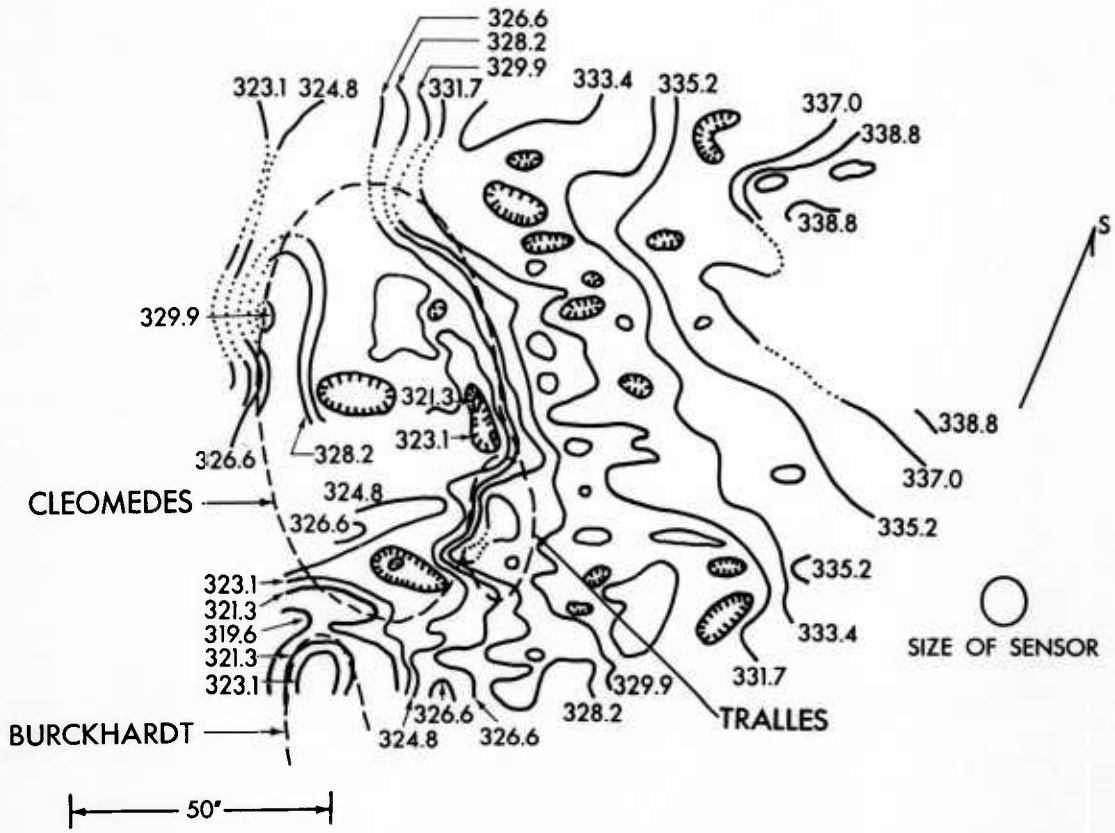

Fig. 12. Isotherms in the Region of Cleomedes September 6, 1960, 7:33 UT

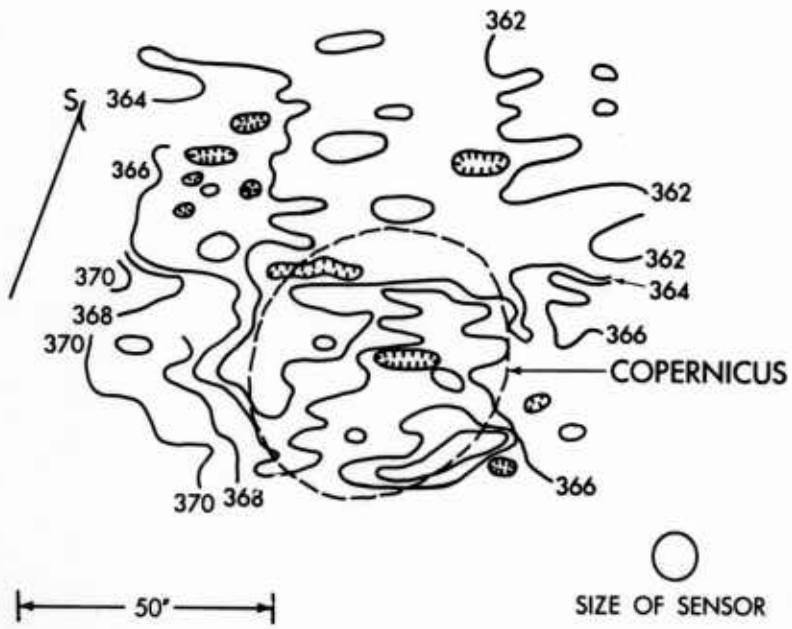

Fig. 13. Isotherms in the Region of Copernicus September 4, 1960, 10:30 UT

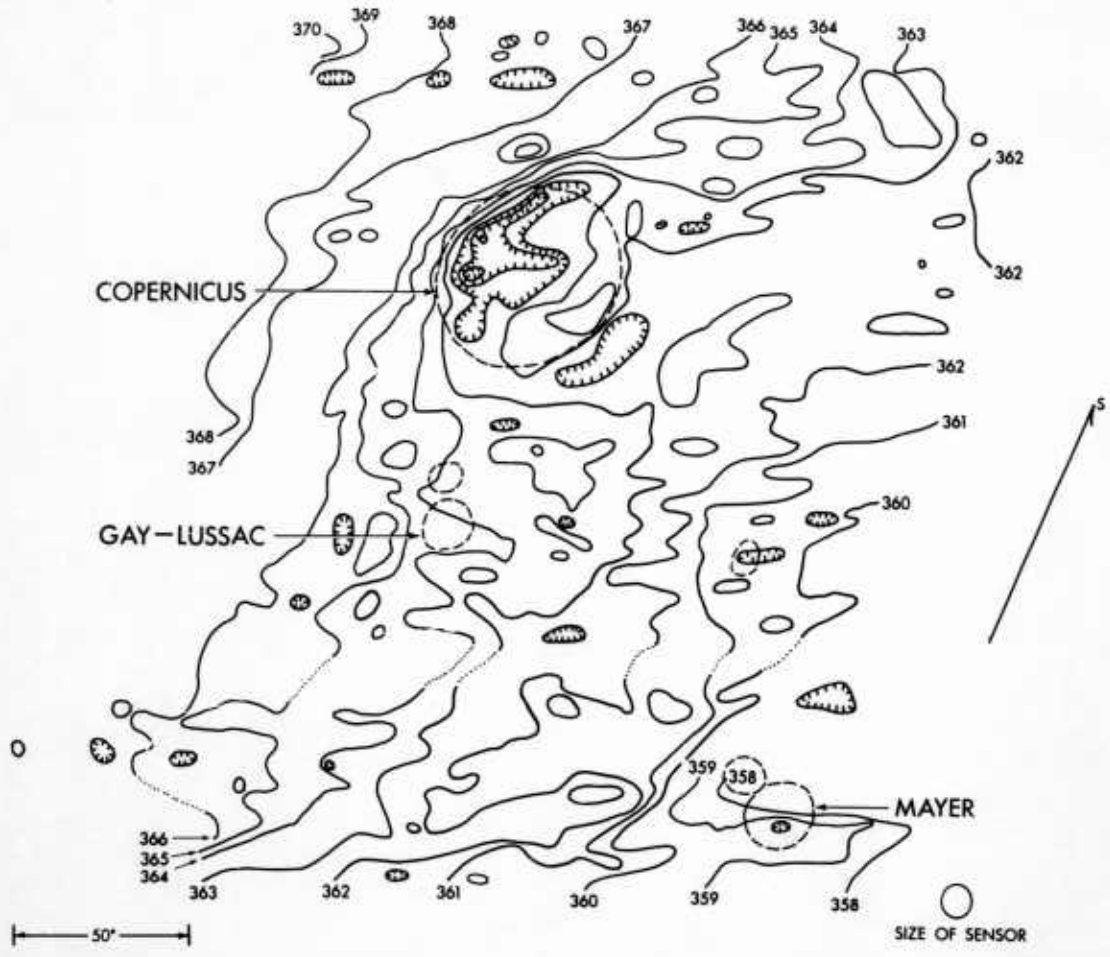

Fig. 14. Isotherms in the Region of Copernicus September 5, 1960, 5:48 UT

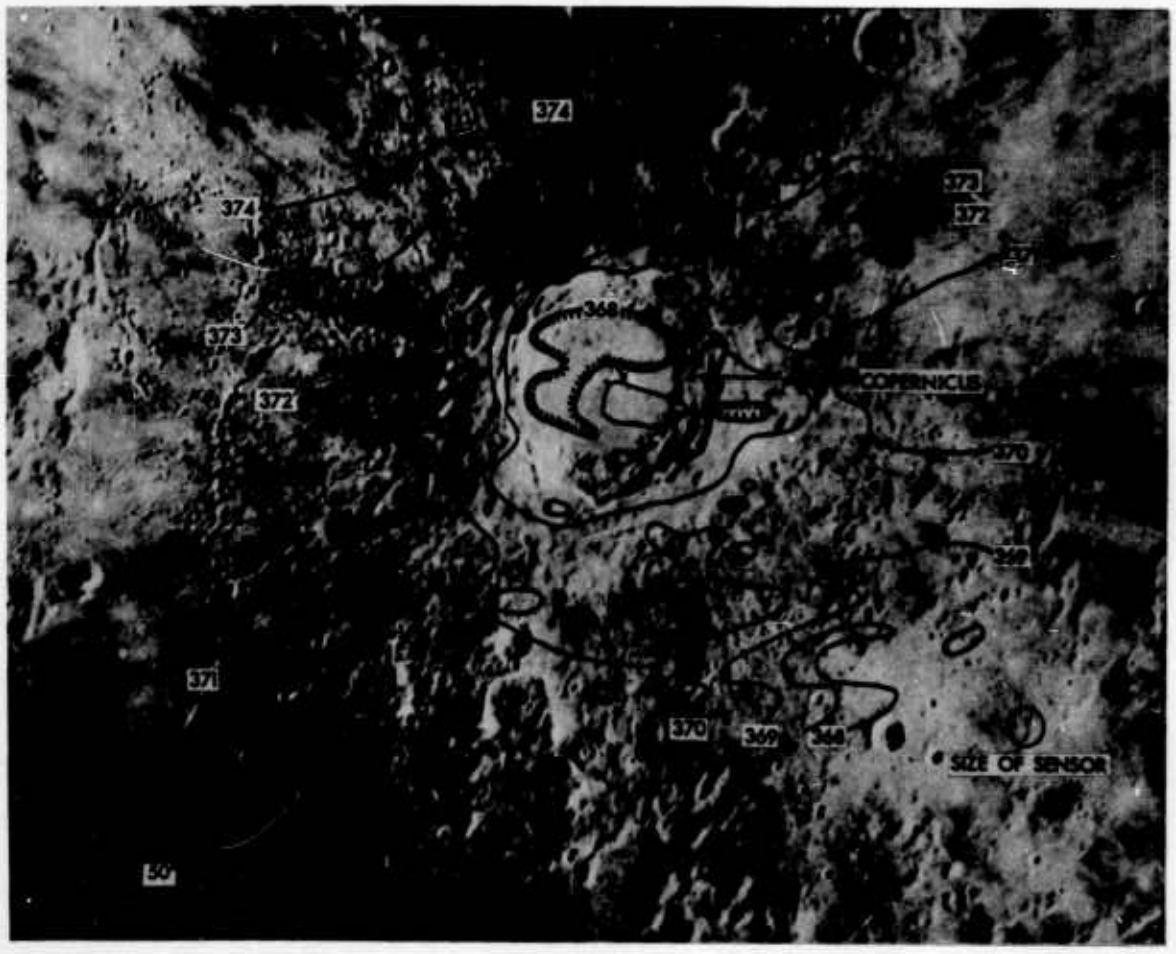

Fig. 15. Isotherms in the Region of Copernicus September 6, 1960, 6:27 UT

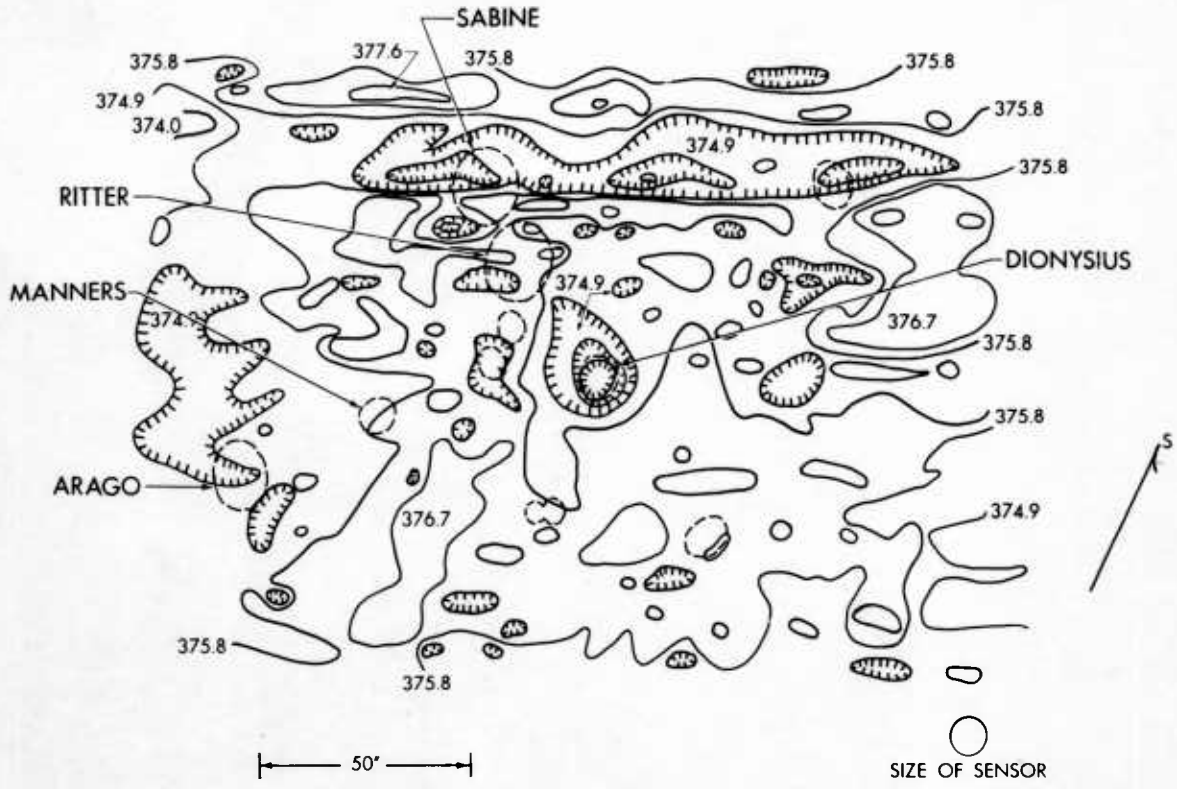

Fig. 16. Isotherms in the Region of Dionysius September 6, 1960, 8:12 UT

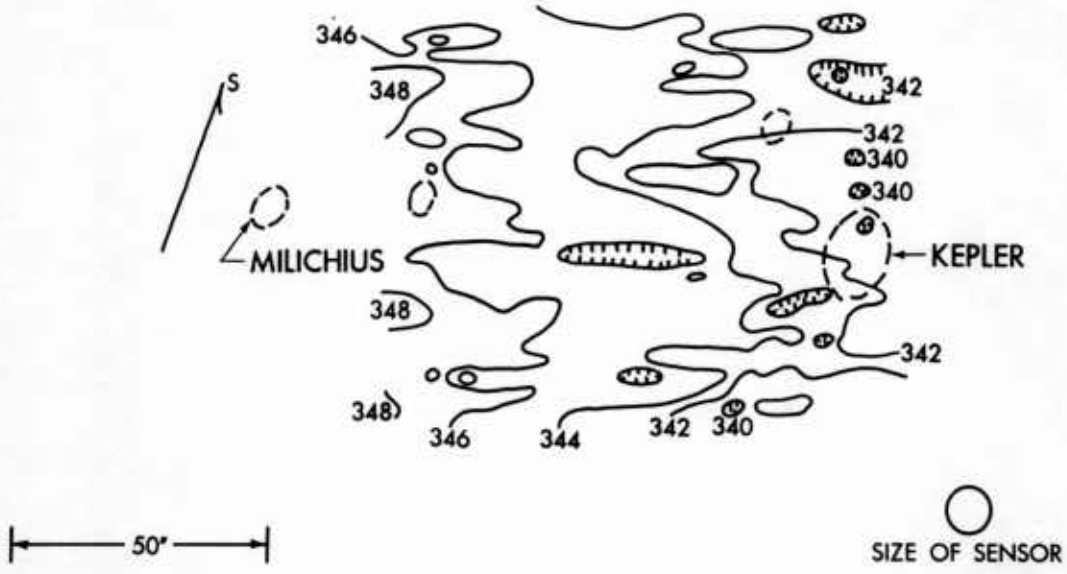

Fig. 17. Isotherms in the Region of Kepler September 4, 1960, 10:37 UT

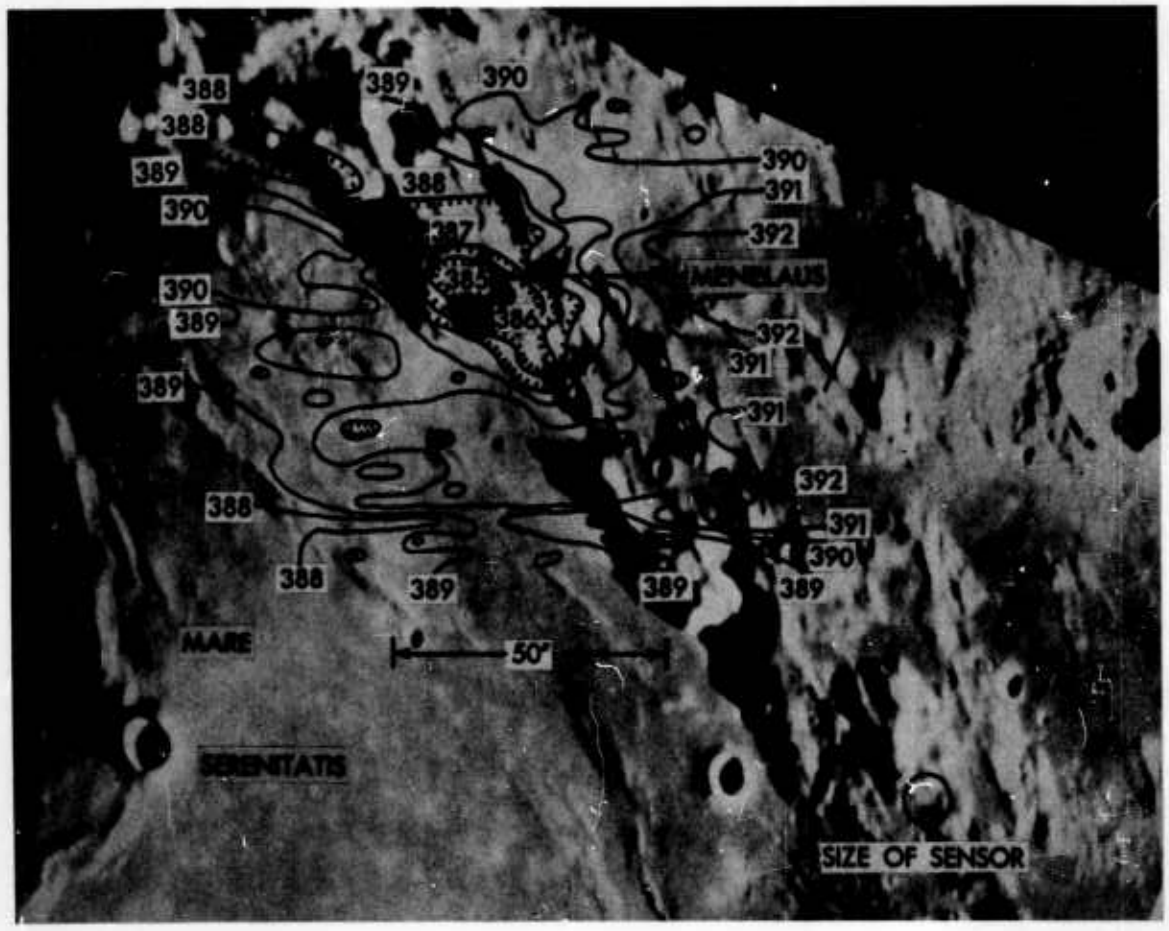

Fig. 18. Isotherms in the Region of Menelaus September 5, 1960, 7:44 UT

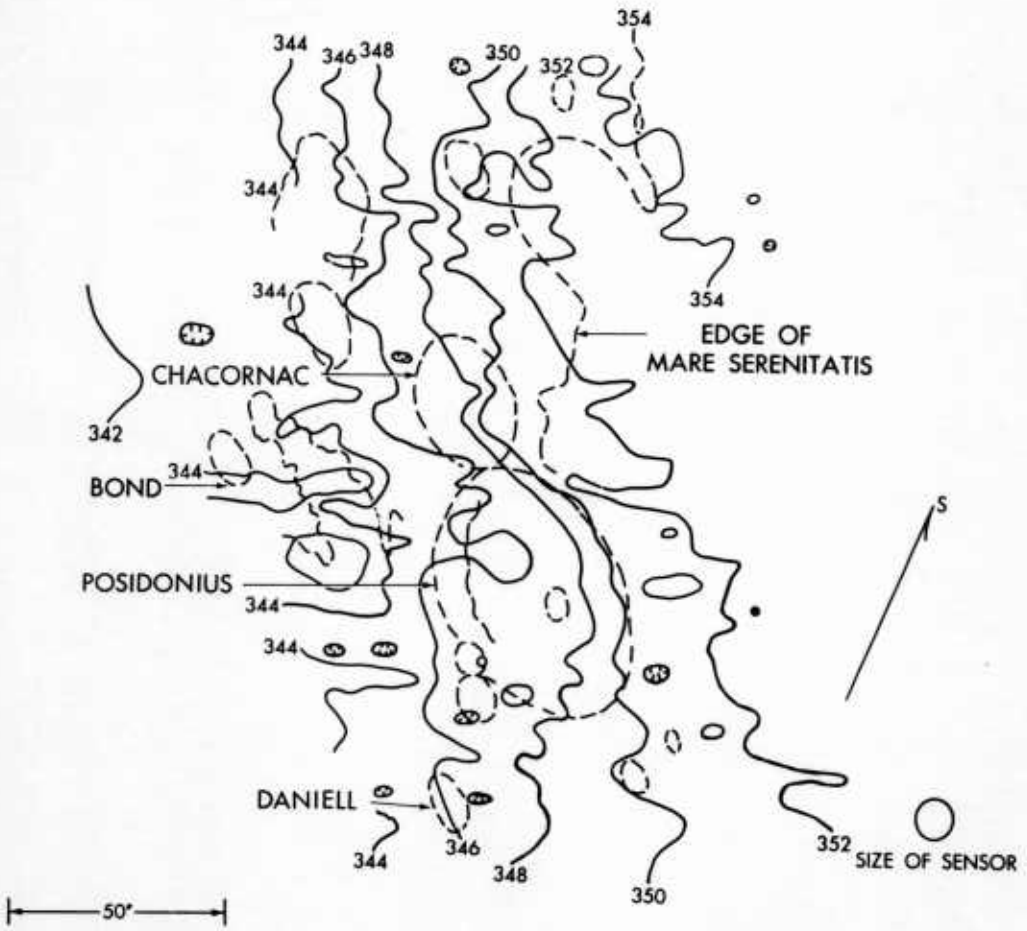

Fig. 19. Isotherms in the Region of Posidonius September 6, 1960, 10:34 UT

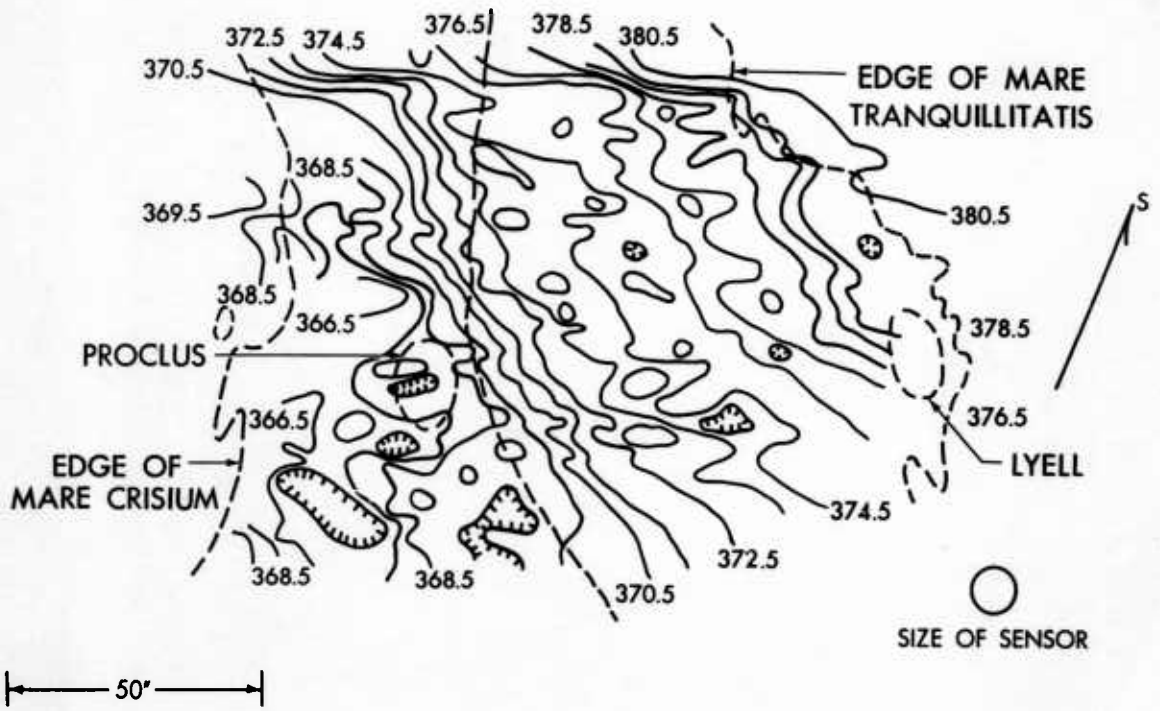

Fig. 20. Isotherms in the Region of Proclus September 5, 1960, 7:20 UT

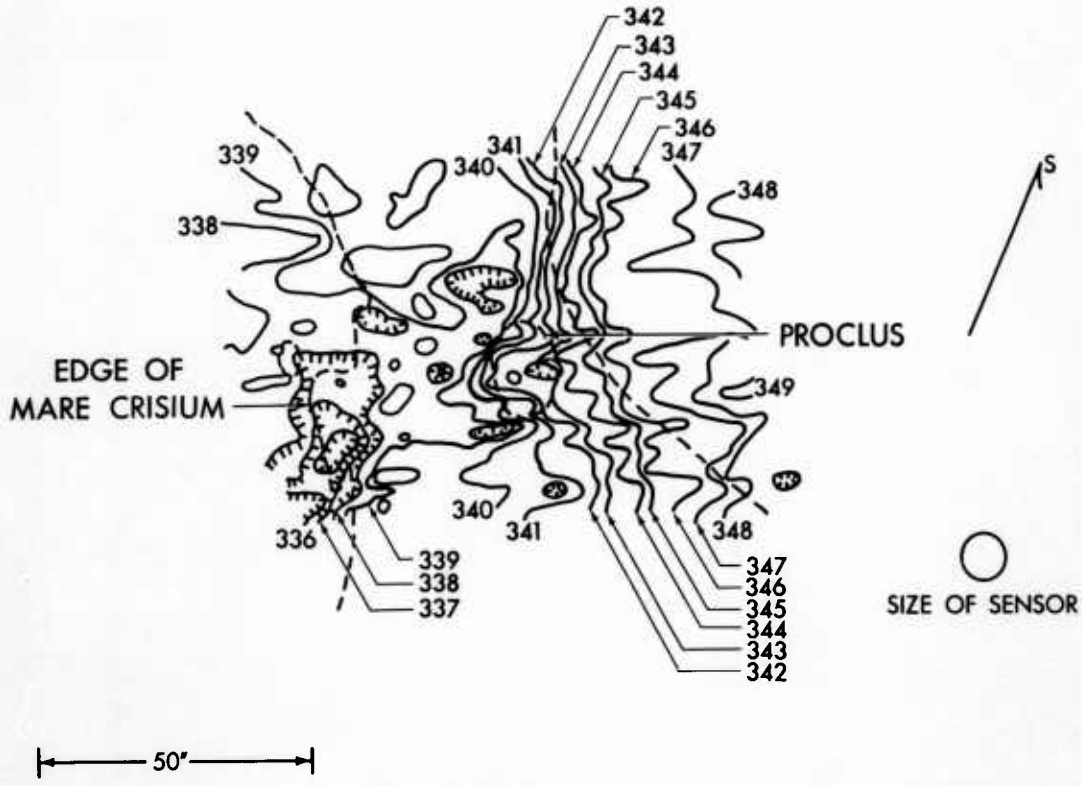

Fig. 21. Isotherms in the Region of Proclus September 6, 1960, 7:54 UT

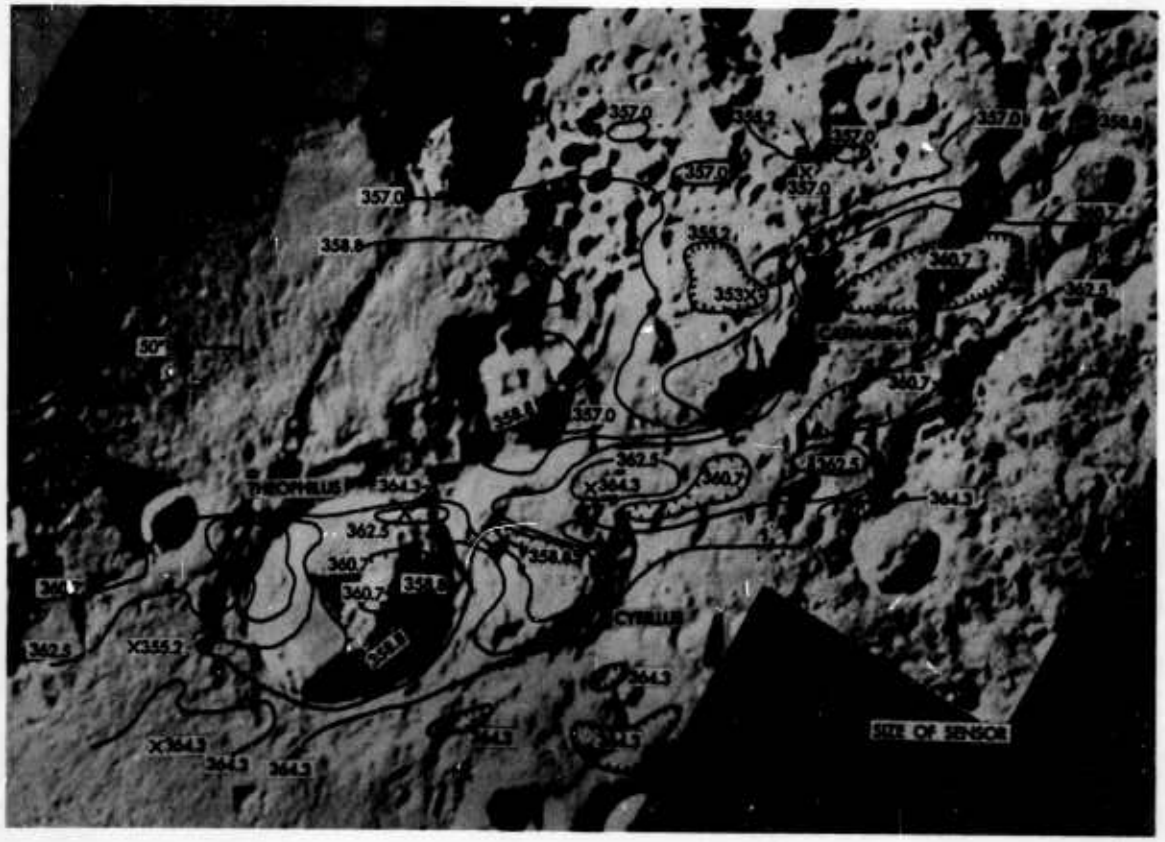

Fig. 22. Isotherms in the Region of Theophilus September 6, 1960, 8:47 UT

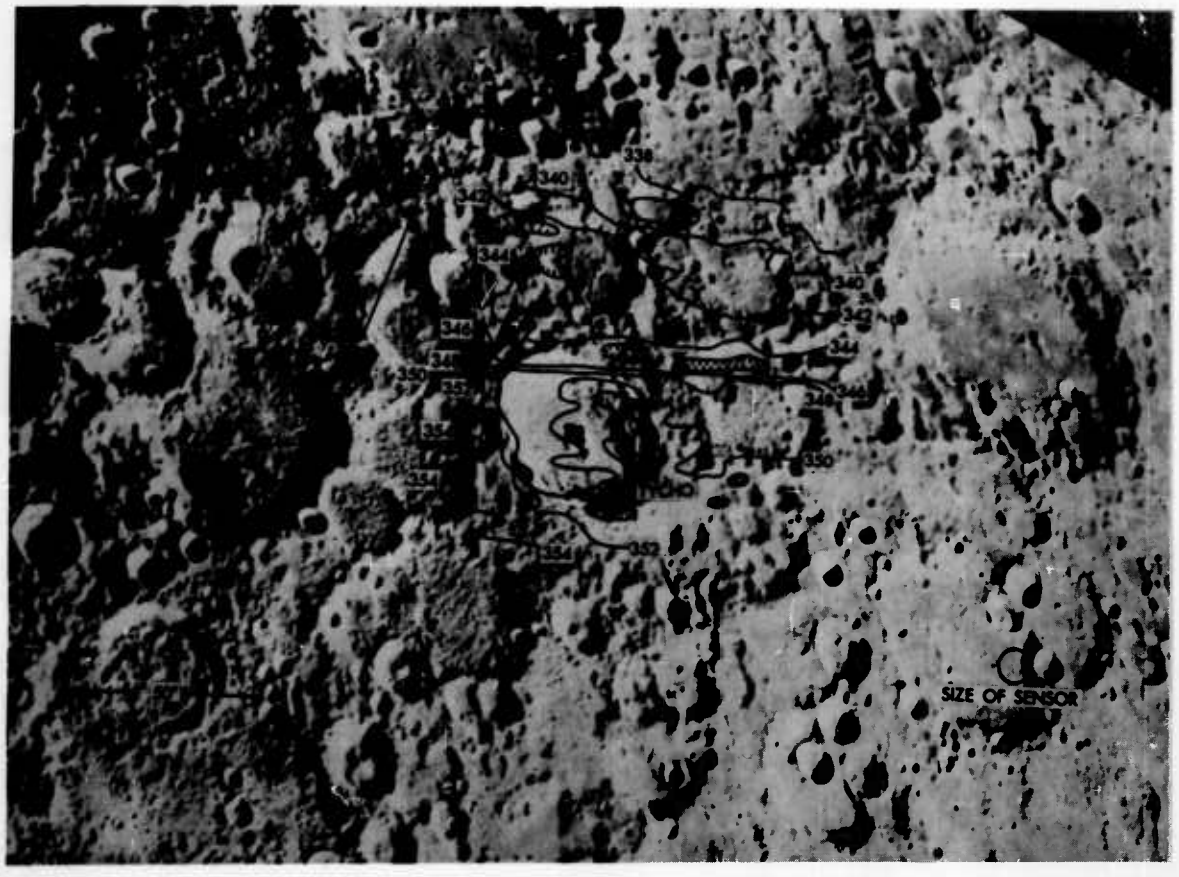

Fig. 23. Isotherms in the Region of Tycho September 4, 1960, 10:08 UT

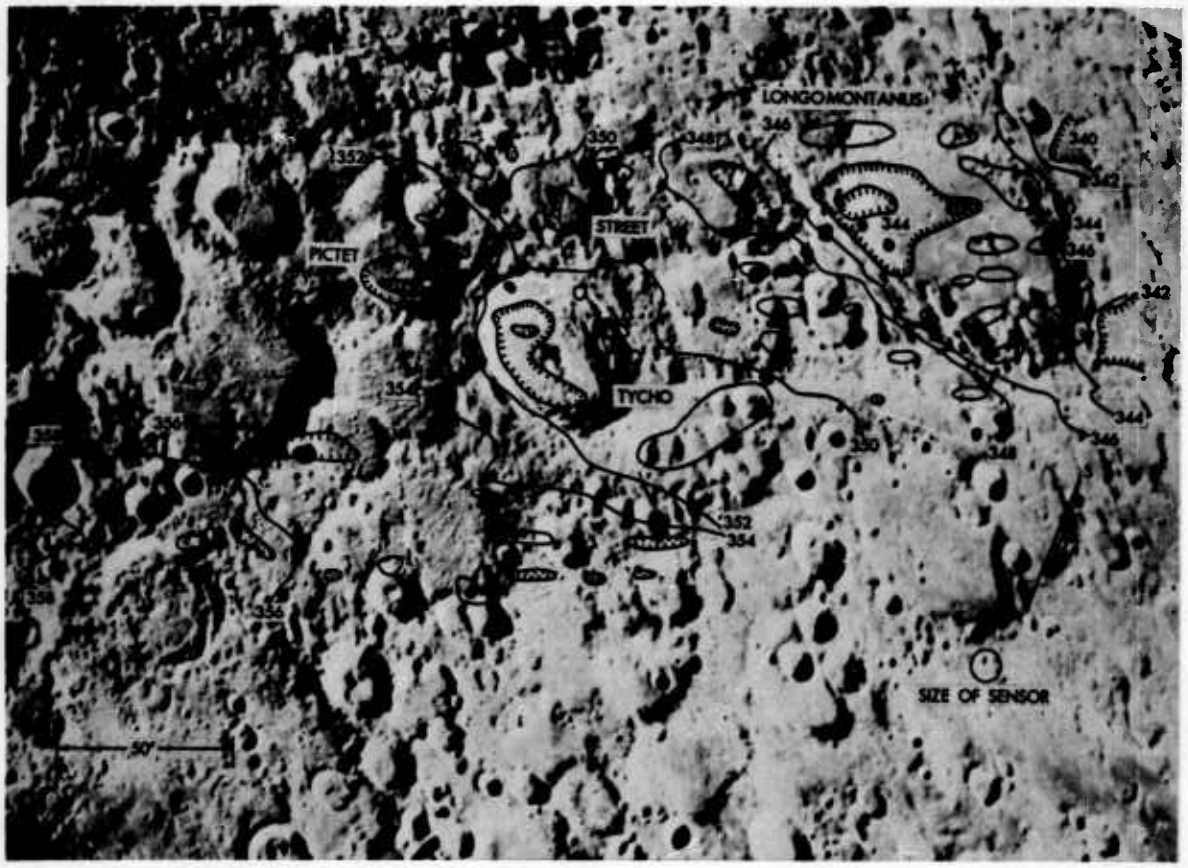

Fig. 24. Isotherms in the Region of Tycho September 5, 1960, 5:18 UT

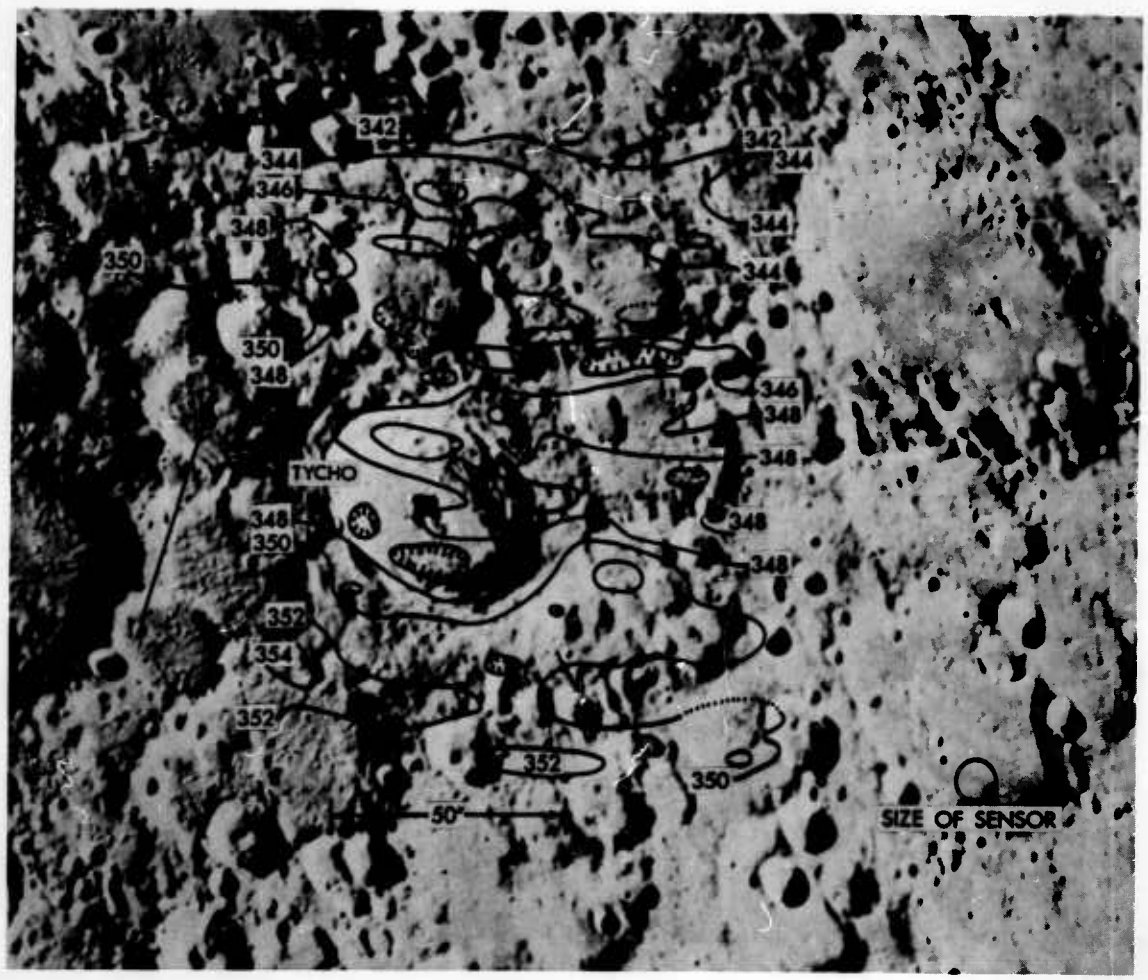

Fig. 25. Isotherms in the Region of Tycho September 6, 1960, 5:50 UT

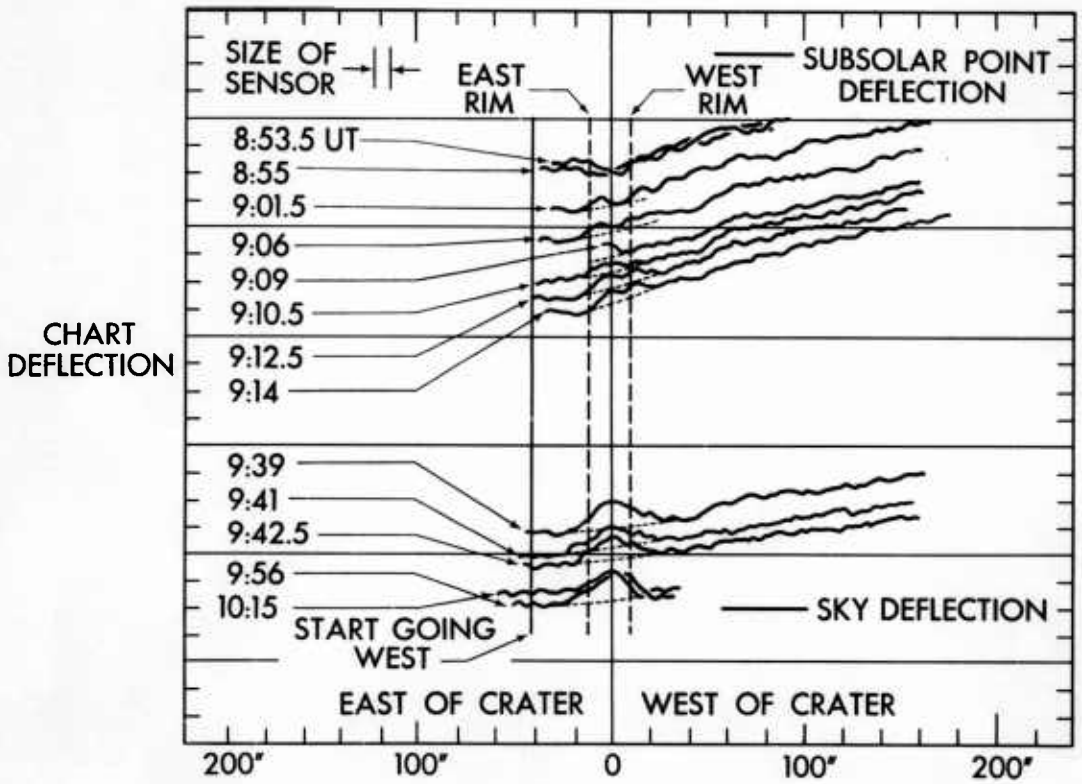

Fig. 26. Temperature Traces Over Aristarchus During Eclipse, September 5, 1960

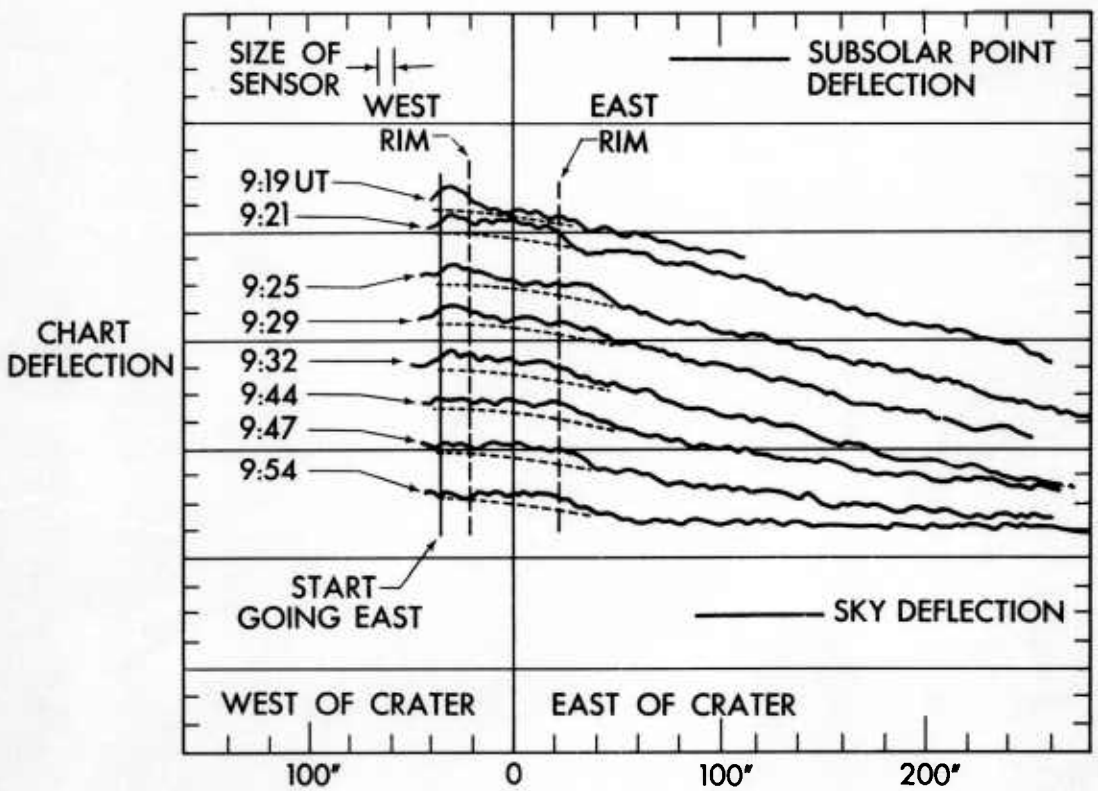

Fig. 27. Temperature Traces Over Copernicus During Eclipse, September 5, 1960

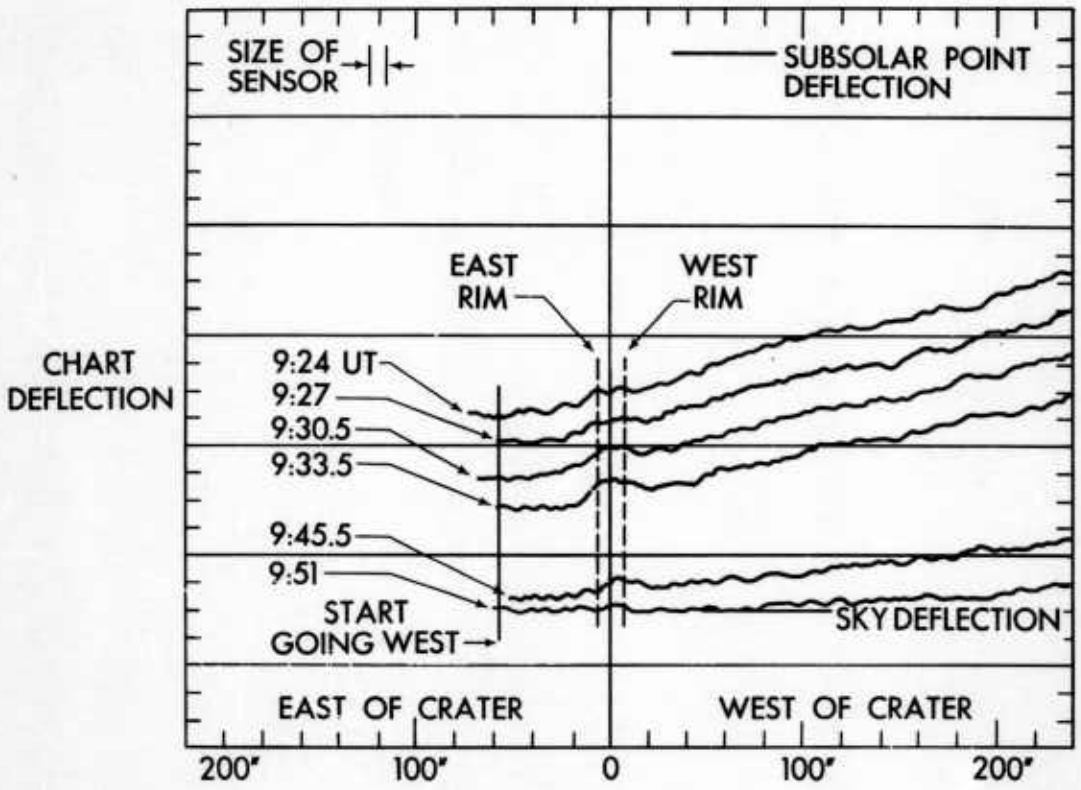

Fig. 28. Temperature Traces Over Kepler During Eclipse, September 5, 1960

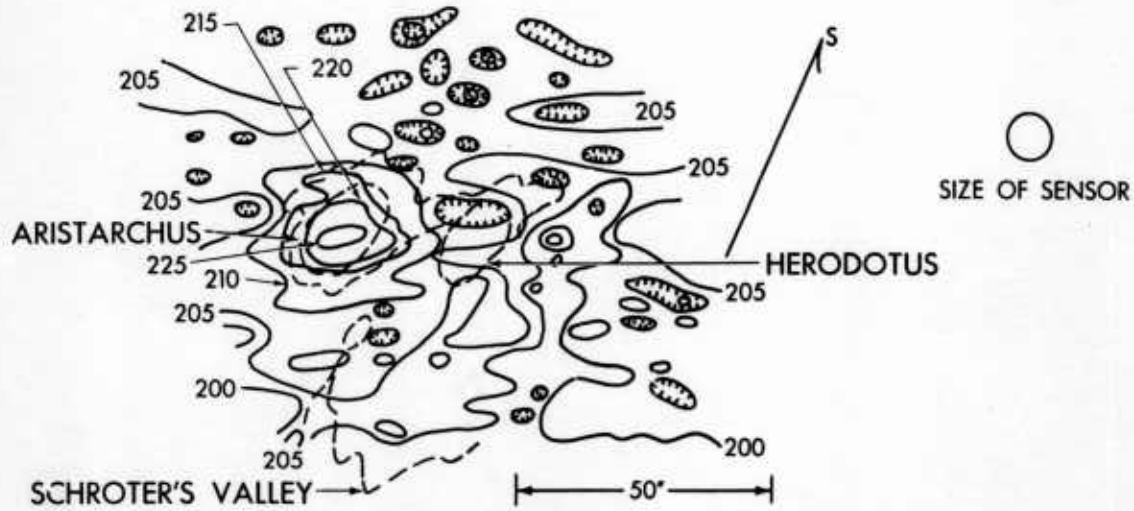

Fig. 29. Isotherms in the Region of Aristarchus During Eclipse, September 5, 1960, 10:12 UT

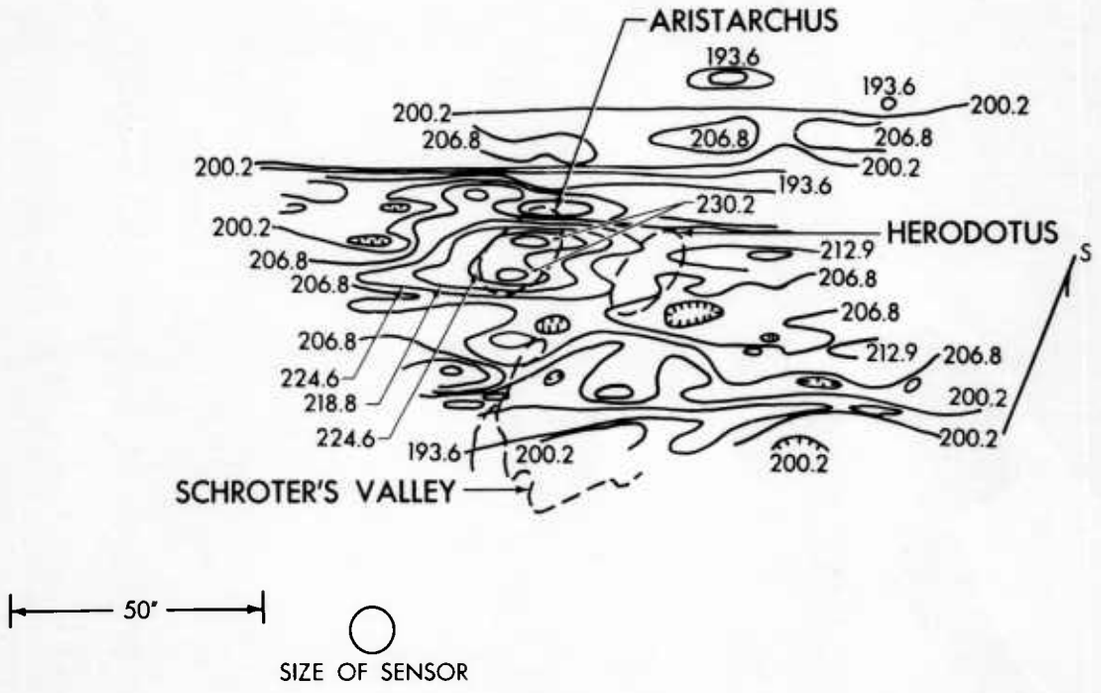

Fig. 30. Isotherms in the Region of Aristarchus During Eclipse, September 5, 1960, 11:04 UT

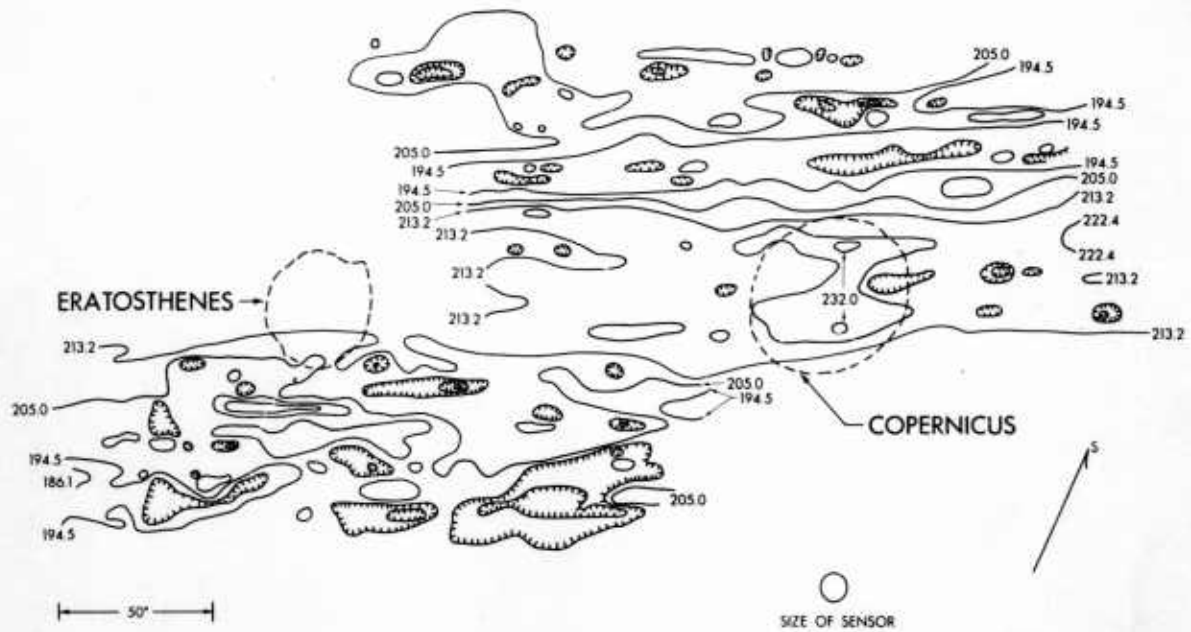

Fig. 31. Isotherms in the Region of Copernicus During Eclipse, September 5, 1960, 11:30 UT

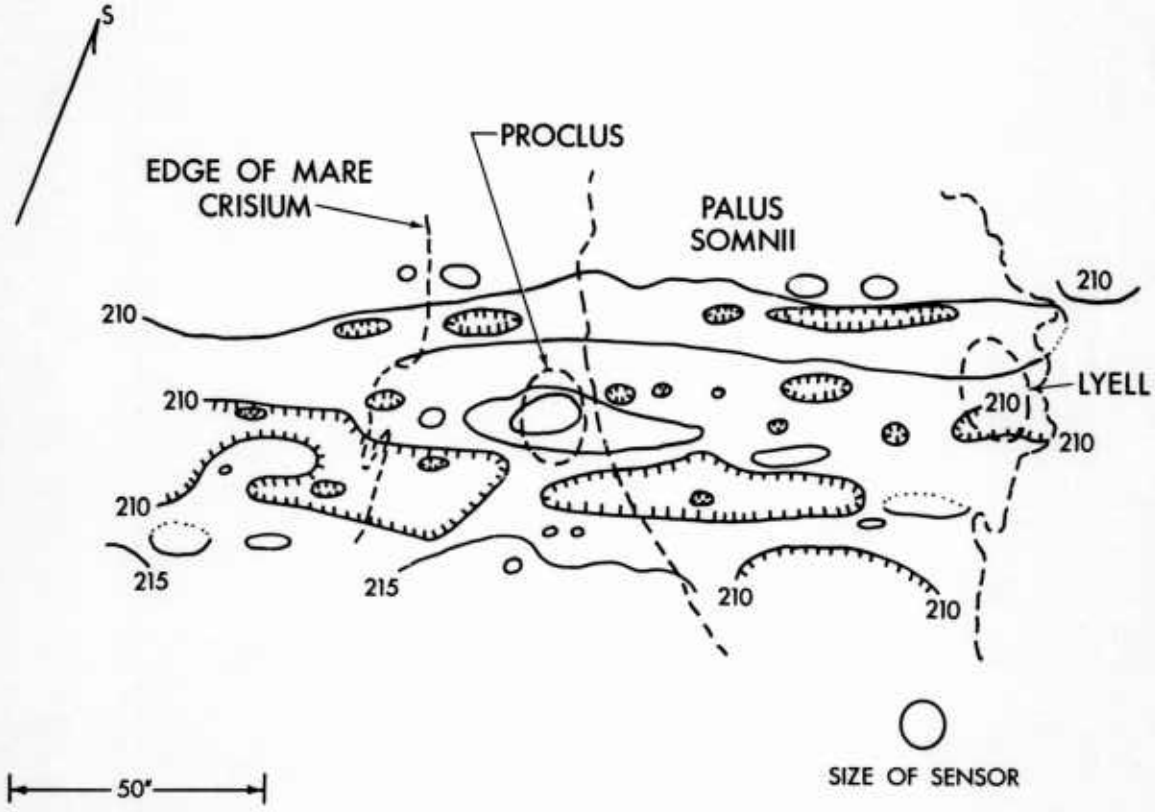

Fig. 32. Isotherms in the Region of Proclus During Eclipse, September 5, 1960, 11:56 UT

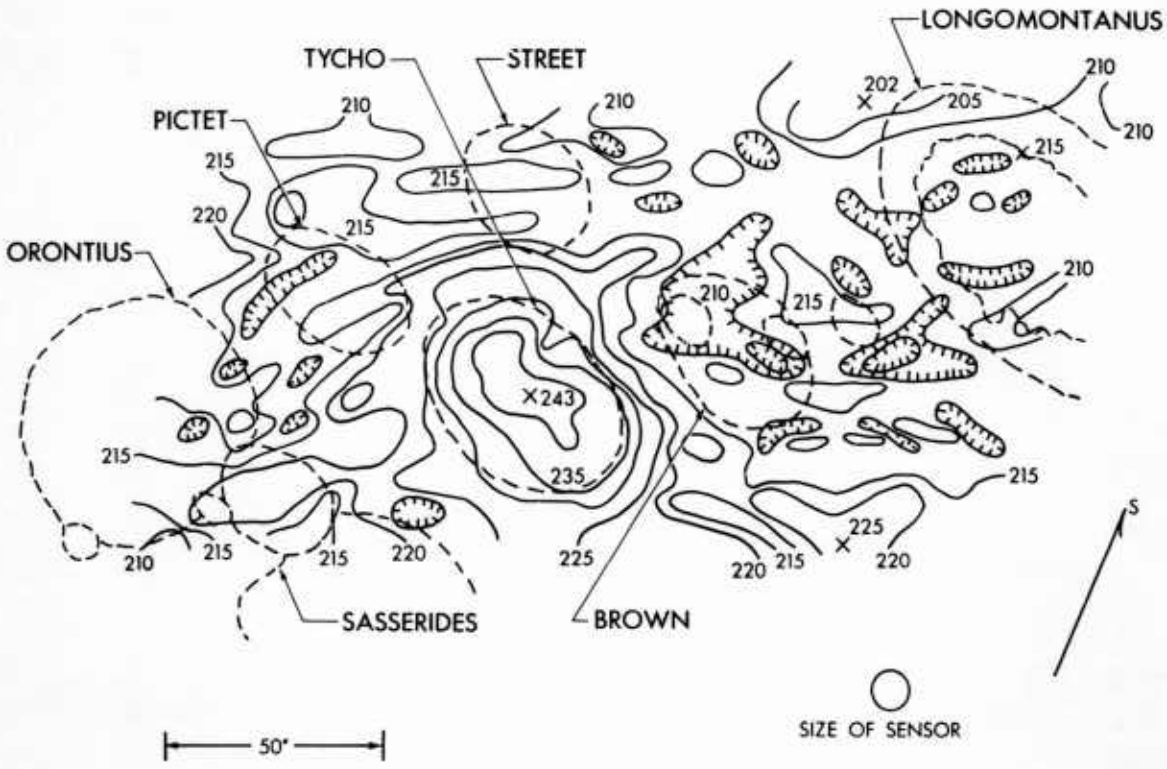

Fig. 33. Isotherms in the Region of Tycho During Eclipse, September 5, 1960, 10:34 UT

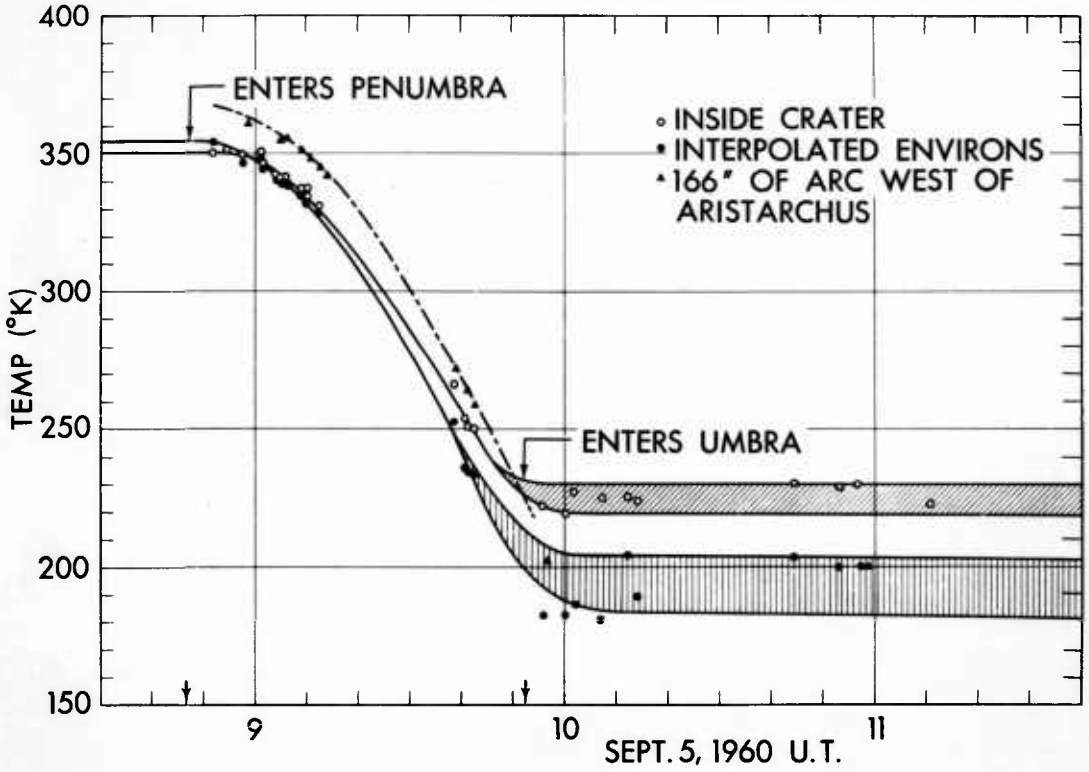

Fig. 34. Eclipse Cooling Curve for the Crater Aristarchus and its Environs

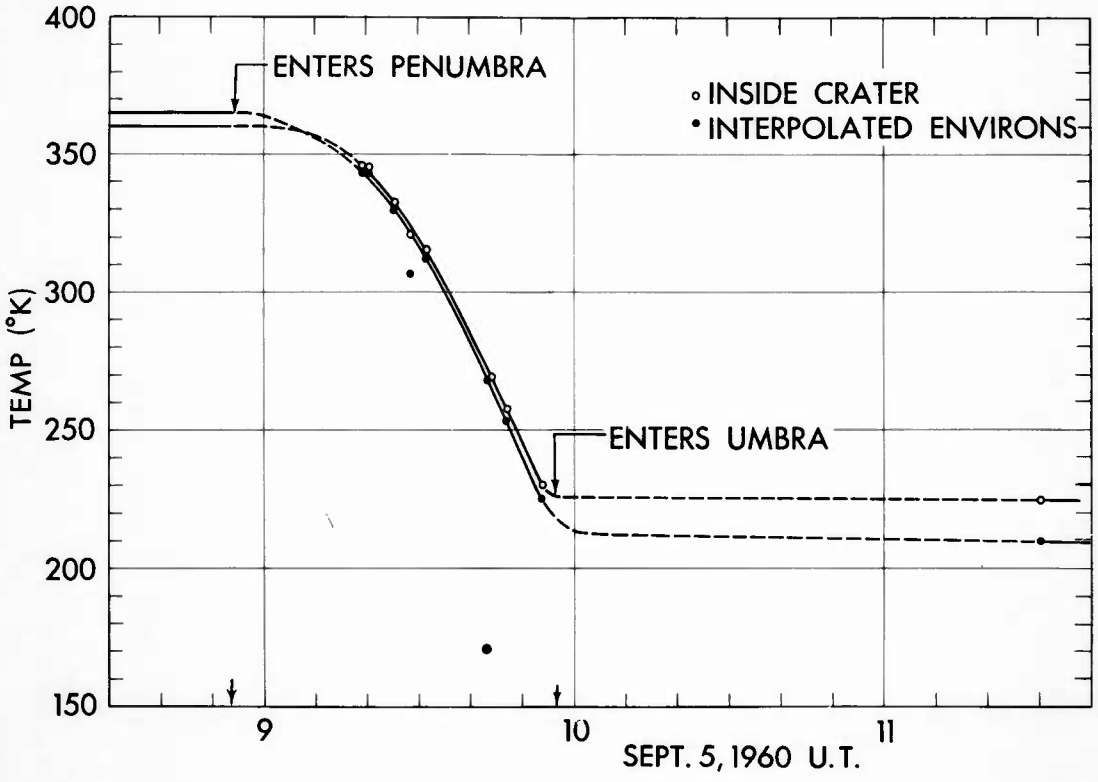

Fig. 35. Eclipse Cooling Curve for the Crater Copernicus and its Environs

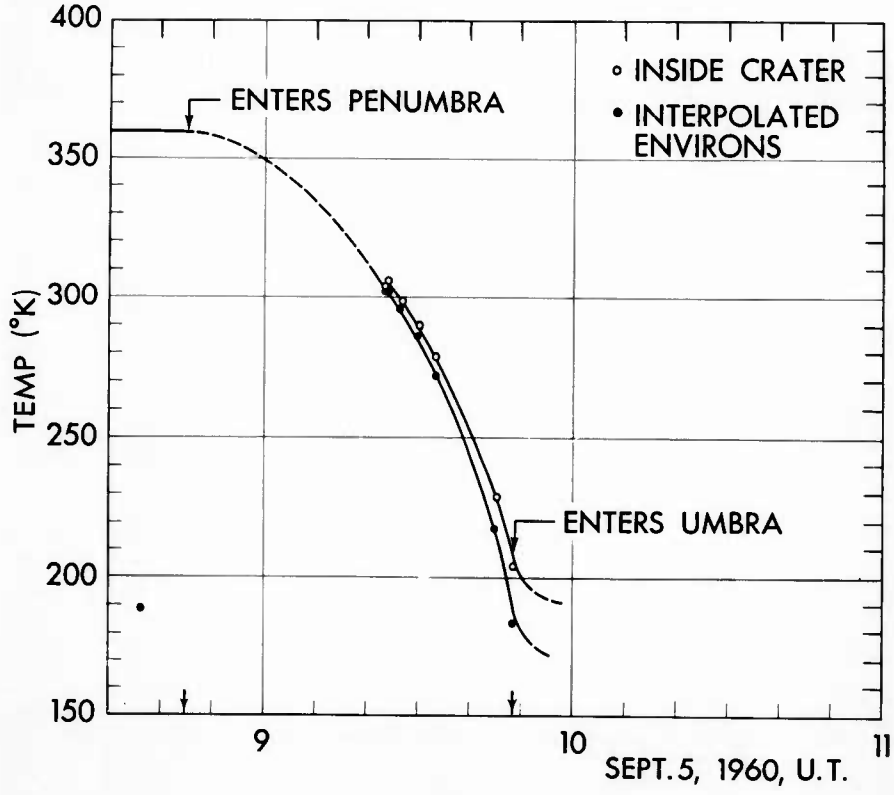

Fig. 36. Eclipse Cooling Curve for the Crater Kepler and its Environs

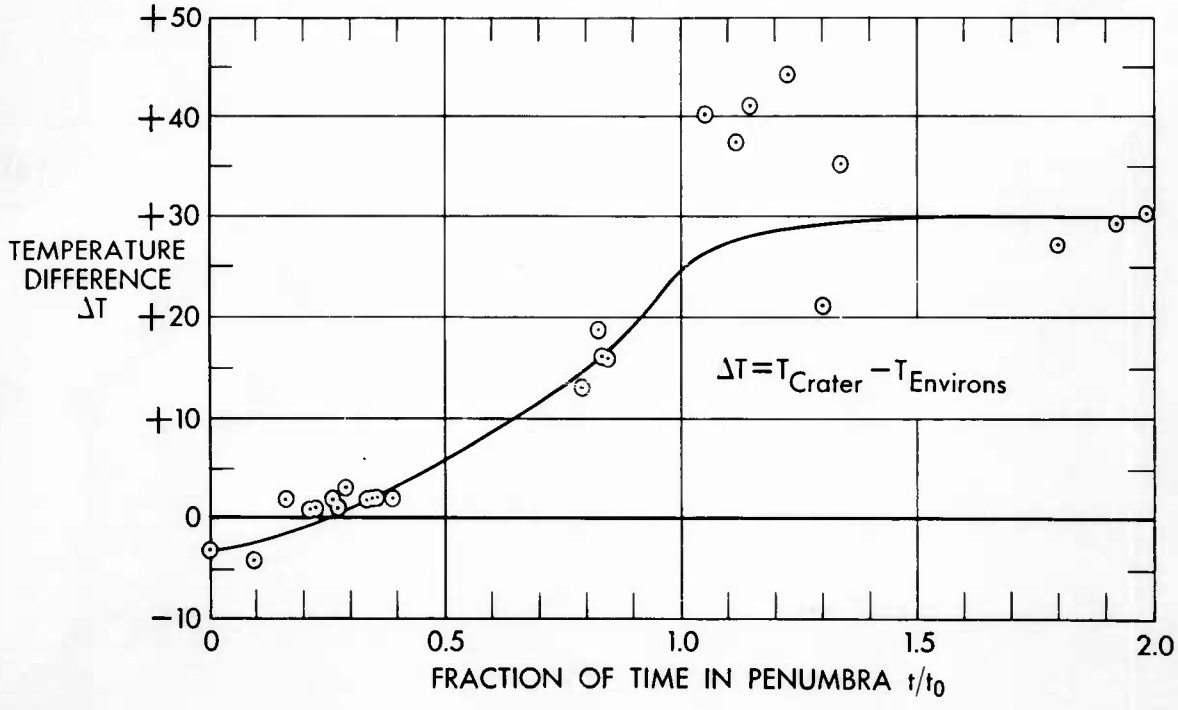

Fig. 37. Difference in Temperatures Between Crater and Interpolated Environs for Aristarchus, September 5, 1960 Eclipse

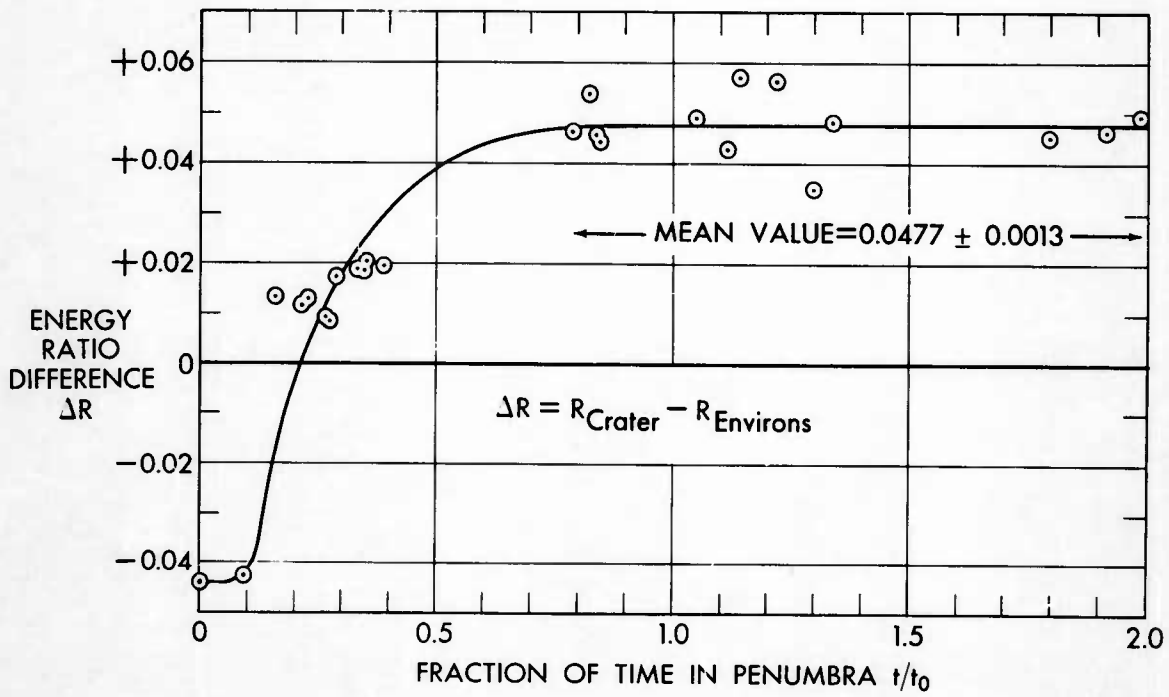

Fig. 38. Diiference in Energy Ratios Between Crater and Interpolated Environs for Aristarchus, September 5, 1960 Eclipse

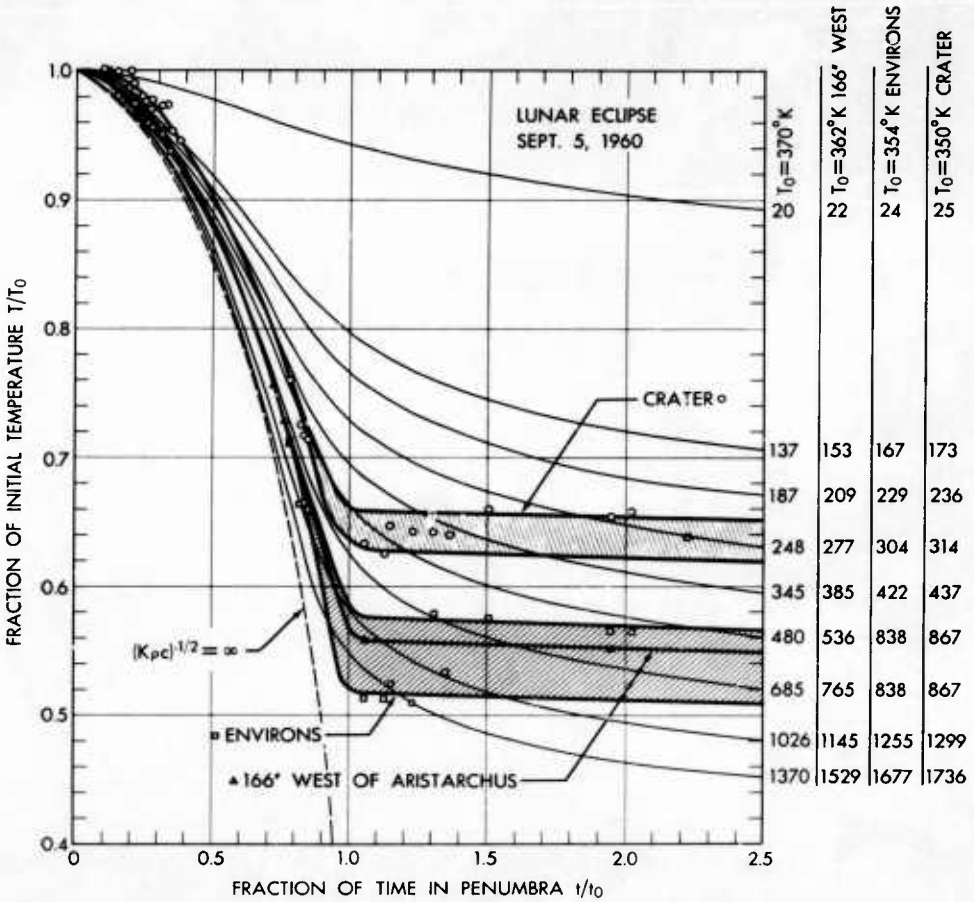

Fig. 39. Normalized Cooling Curves for Aristarchus and its Environs, Experimental Values and Theoretical Homogeneous Surface With Different Values of $(K\rho c)^{-1/2}$

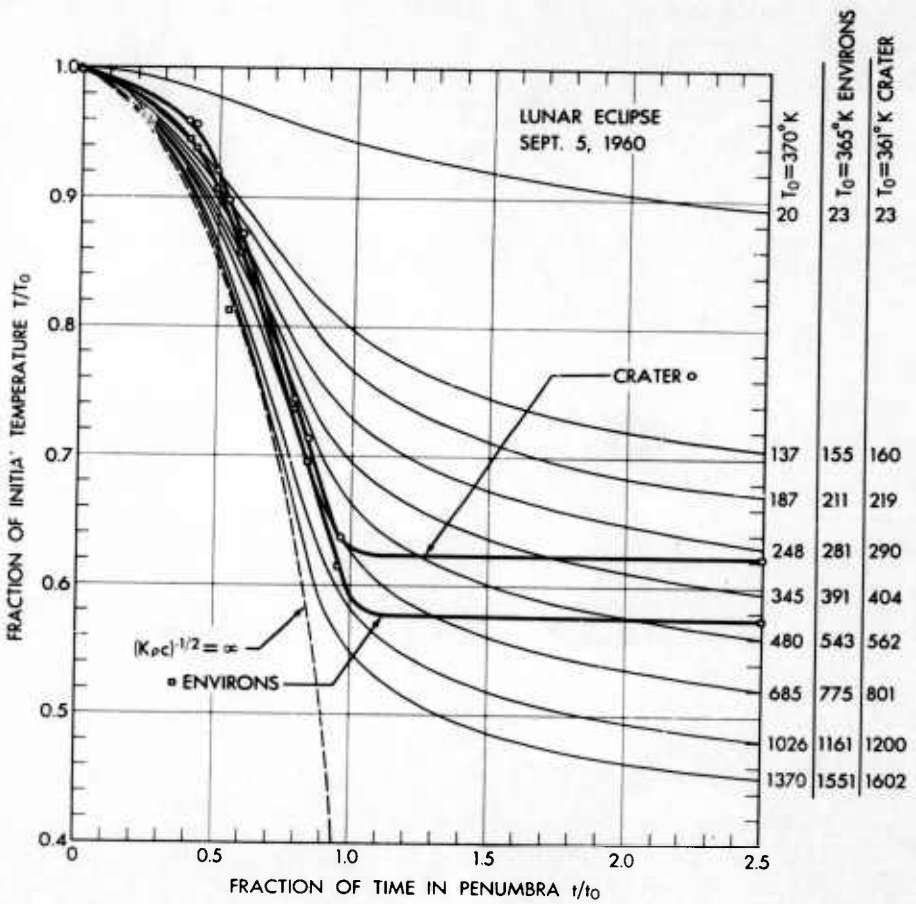

Fig. 40. Normalized Cooling Curves for Copernicus and its Environs, Experimental Values and Theoretical Homogeneous Surface With Different Values of $(K\rho c)^{-1/2}$

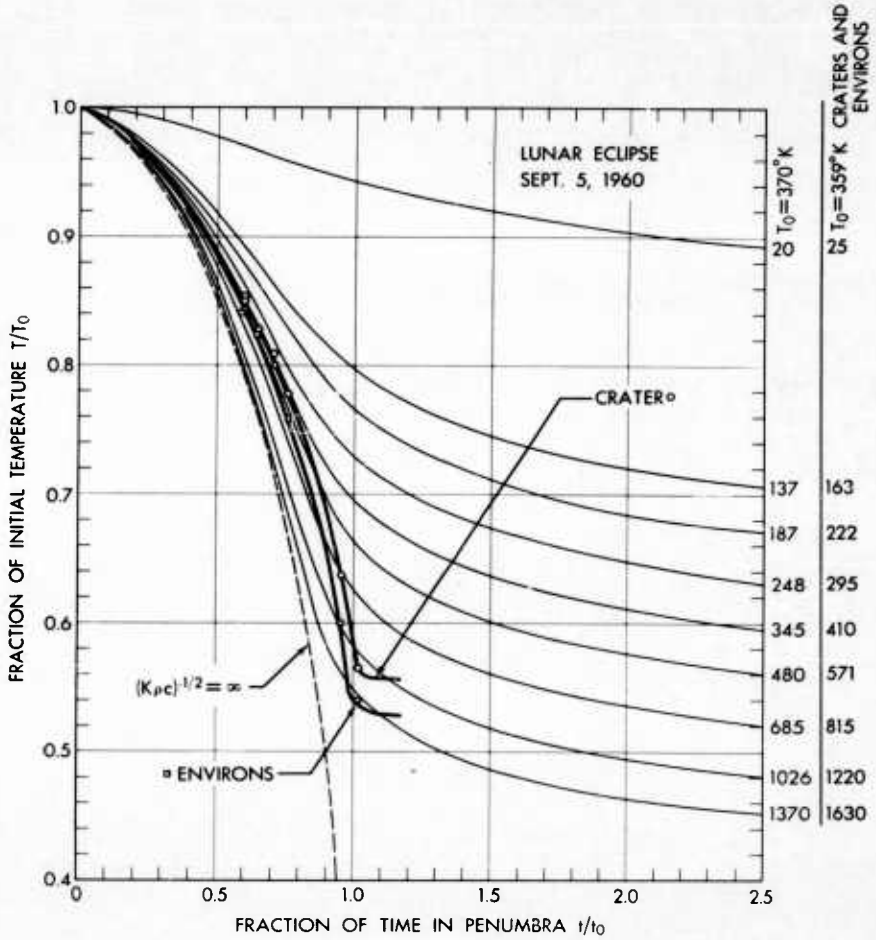

Fig. 41. Normalized Cooling Curves for Kepler and its Environs, Experimental Va ues and Theoretical Homogeneous Surface With Different Values of $(K\rho c)^{-1/2}$

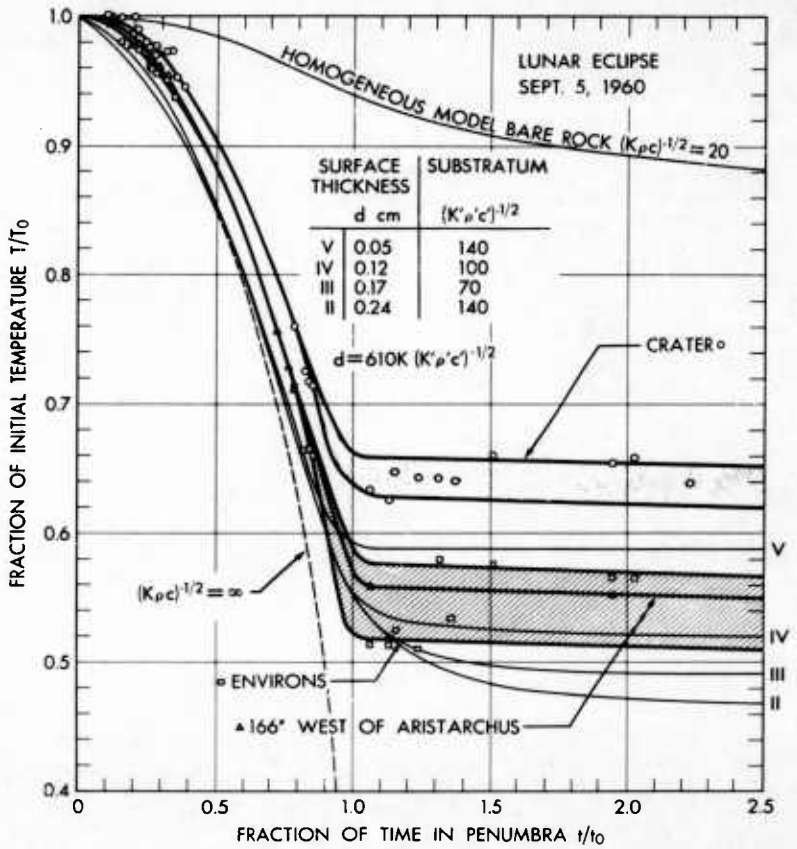

Fig. 42. Normalized Cooling Curve for Aristarchus and its Environs, Experimental Values and Theoretical Two-layer Model

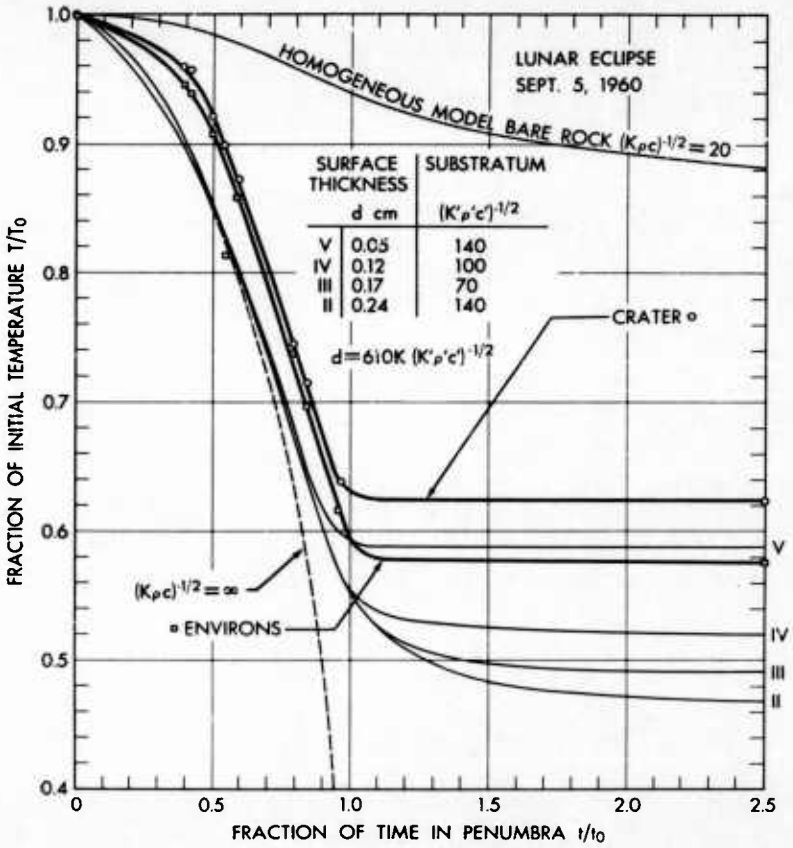

Fig. 43. Normalized Cooling Curve for Copernicus and its Environs, Experimental Values and Theoretical Two-layer Model

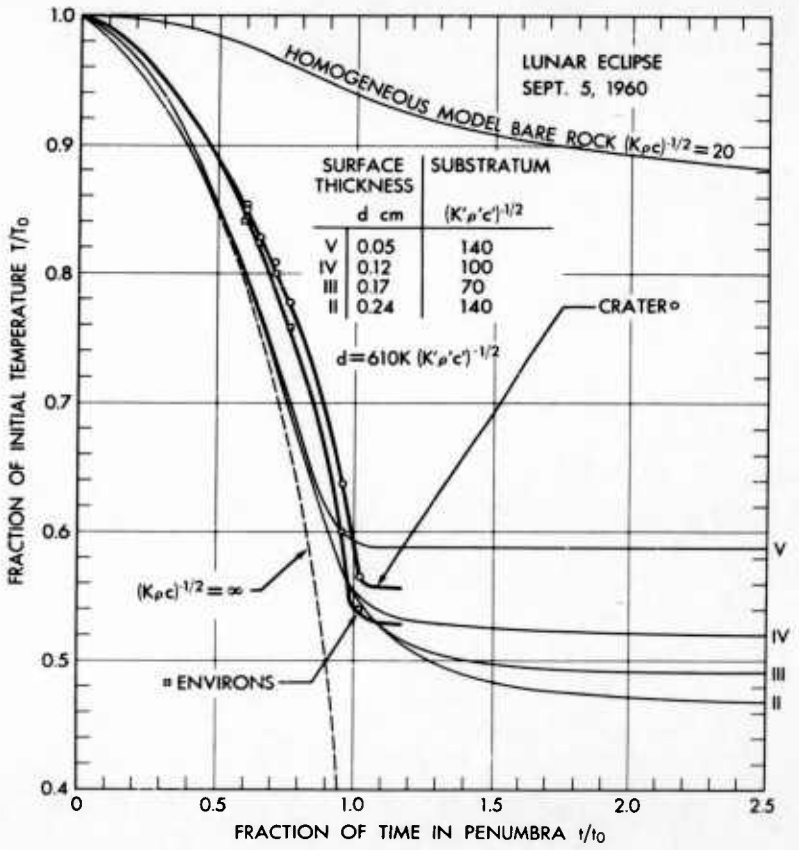

Fig. 44. Normalized Cooling Curve for Kepler and its Environs, Experimental Values and Theoretical Two-layer Model

UNCLASSIFIED